

1 **TITLE**

2 Inherited *MUTYH* mutations cause elevated somatic mutation rates and distinctive mutational  
3 signatures in normal human cells

4  
5 **AUTHORS**

6 Philip S. Robinson<sup>1,2</sup>, Laura E. Thomas<sup>3</sup>, Federico Abascal<sup>1</sup>, Hyunchul Jung<sup>1</sup>, Luke M.R. Harvey<sup>1</sup>, Hannah  
7 D. West<sup>4</sup>, Sigurgeir Olafsson<sup>1</sup>, Bernard C. H. Lee<sup>1,5</sup>, Tim H.H. Coorens<sup>1</sup>, Henry Lee-Six<sup>1</sup>, Laura Butlin<sup>4</sup>,  
8 Nicola Lander<sup>4</sup>, Mathijs A. Sanders<sup>1,6</sup>, Stefanie V. Lensing<sup>1</sup>, Simon J.A. Buczacki<sup>7</sup>, Rogier ten Hoopen<sup>8</sup>,  
9 Nicholas Coleman<sup>9,10</sup>, Roxanne Brunton-Sim<sup>11</sup>, Simon Rushbrook<sup>11,12</sup>, Kourosh Saeb-Parsy<sup>13,14</sup>, Fiona  
10 Laloo<sup>15</sup>, Peter J. Campbell<sup>1</sup>, Iñigo Martincorena<sup>1</sup>, Julian R. Sampson<sup>4</sup>, Michael R. Stratton<sup>1\*</sup>

11  
12 **AFFILIATIONS**

13 1. Cancer, Ageing and Somatic Mutation (CASM), Wellcome Sanger Institute, Hinxton, CB10 1SA,  
14 UK.

15 2. Department of Paediatrics, University of Cambridge, Cambridge, CB2 0QQ, UK.

16 3. Institute of Life Science, Swansea University, Swansea, SA28PP, UK.

17 4. Institute of Medical Genetics, Division of Cancer and Genetics, Cardiff University School of  
18 Medicine, Cardiff, UK.

19 5. Hereditary Gastrointestinal Cancer Genetic Diagnosis Laboratory, Department of Pathology,  
20 The University of Hong Kong, Queen Mary Hospital, Pokfulam, Hong Kong

21 6. Department of Haematology, Erasmus University Medical Centre, 3015 CN, Rotterdam, The  
22 Netherlands

23 7. Nuffield Department of Surgical Sciences, Medical Sciences Division, University of Oxford,  
24 Oxford, UK.

25 8. Department of Oncology, University of Cambridge, Cambridge, UK.

26 9. Department of Pathology, University of Cambridge, Cambridge, UK.

27 10. Cambridge University Hospitals NHS Foundation Trust, Cambridge, UK.

28 11. Norfolk and Norwich University Hospital, Norwich, UK.

29 12. Norwich Medical School, University of East Anglia, Norwich, UK.

30 13. Department of Surgery, University of Cambridge, Cambridge, UK.

31 14. Cambridge NIHR Biomedical Research Centre, Cambridge Biomedical Campus, Cambridge,  
32 UK.

33 15. Manchester Centre for Genomic Medicine, Saint Marys Hospital, Oxford Road, Manchester,  
34 UK.

35  
36 \* Corresponding author [mrs@sanger.ac.uk](mailto:mrs@sanger.ac.uk)

38

39

40 **Summary**

41

42 **KEYWORDS**

43 Somatic mutations, normal tissues, genomics, ageing, mutational signatures, DNA repair

44

45 **ABSTRACT**

46

47 Cellular DNA damage caused by reactive oxygen species is repaired by the base excision repair (BER)  
48 pathway which includes the DNA glycosylase *MUTYH*. Inherited biallelic *MUTYH* mutations cause  
49 predisposition to colorectal adenomas and carcinoma. However, the mechanistic progression from  
50 germline *MUTYH* mutations to **MUTYH-Associated Polyposis (MAP)** is incompletely understood. Here,  
51 we sequenced normal tissue DNAs from 10 individuals with MAP. Somatic base substitution mutation  
52 rates in intestinal epithelial cells were elevated 2 to 5-fold in all individuals, except for one showing a  
53 33-fold increase, and were also increased in other tissues. The increased mutation burdens were of  
54 multiple mutational signatures characterised by C>A changes. Different mutation rates and signatures  
55 between individuals were likely due to different *MUTYH* mutations or additional inherited mutations  
56 in other BER pathway genes. The elevated base substitution rate in normal cells likely accounts for the  
57 predisposition to neoplasia in MAP. Despite ubiquitously elevated mutation rates, individuals with  
58 MAP do not display overt evidence of premature ageing. Thus, accumulation of somatic mutations  
59 may not be sufficient to cause the global organismal functional decline of ageing.

60

61 **INTRODUCTION**

62  
63 The genomes of all normal human cells are thought to acquire mutations during the course of life.  
64 However, the mutation rates of normal cells and the processes of DNA damage, repair and replication  
65 that underlie them are incompletely understood<sup>1-8</sup>. A ubiquitous source of potential mutations is DNA  
66 damage caused by reactive oxygen species (ROS) which are formed as by-products of aerobic  
67 metabolism<sup>9</sup>. ROS cause a variety of DNA lesions, the most common being 8-oxoguanine (8-OG)<sup>10</sup>. As  
68 a consequence of mispairing with adenine during DNA replication, 8-OG can cause G:C>T:A (referred  
69 to as C>A for brevity) transversion mutations<sup>11</sup>. Under normal circumstances, 8-OG and its  
70 consequences are efficiently mitigated by the Base Excision Repair (BER) pathway effected by DNA  
71 glycosylases; oxoguanine DNA glycosylase (OGG1) removes 8-OG<sup>12</sup> and MutY DNA glycosylase  
72 (MUTYH) removes adenines misincorporated opposite 8-OG<sup>13</sup>.

73  
74 Mutations in *MUTYH* engineered in experimental systems can impair its glycosylase activity, reducing  
75 its ability to excise mispaired bases and leading to an increased rate of predominantly C>A mutations<sup>14-18</sup>. *MUTYH*  
76 mutations inherited in the germline in humans cause an autosomal recessive syndrome  
77 (*MUTYH*-associated polyposis, MAP) characterised by intestinal adenomatous polyposis and an  
78 elevated risk of early onset colorectal and duodenal cancer<sup>19-22</sup>. The age of onset and the burden of  
79 intestinal polyps are highly variable between individuals, ranging from 10s to 100s leading to a  
80 substantially increased incidence of colorectal cancer.<sup>23-27</sup> Risks of other cancer types are also thought  
81 to be increased<sup>28</sup>.

82  
83 Colorectal adenomas and carcinomas from individuals with MAP show a predominance of C>A  
84 mutations consistent with the presence of an elevated mutation rate attributed to defective *MUTYH*  
85 function<sup>29-33</sup>. However, whether there is an increased mutation rate in normal cells from individuals  
86 with biallelic germline *MUTYH* mutations is unknown. If present in normal cells, understanding the  
87 magnitude of the increase in mutation rate, the tissues and cell types in which it occurs, the proportion  
88 of cells which show it, the mutational processes responsible and the effects of early neoplastic change  
89 would provide insight into the genesis of the elevated cancer risk observed in these individuals. In this  
90 study we characterise the somatic mutation rates and mutational signatures of normal intestinal cells,  
91 and other normal cells, from individuals with MAP.

92  
93 **RESULTS**

94 **Clinical information**

95 Ten individuals aged 16 to 79 years with biallelic germline *MUTYH* mutations were studied. These  
96 included five missense mutation homozygotes (four *MUTYH*<sup>Y179C+/+</sup>, one *MUTYH*<sup>G286E+/+</sup>), three  
97 compound heterozygotes for the same pair of missense mutations (*MUTYH*<sup>Y179C+/-;G396D+/-</sup>), and two  
98 siblings homozygous for a nonsense mutation (*MUTYH*<sup>Y104\*+/+</sup>). These *MUTYH* germline mutations have  
99 all been previously recognised as predisposing to MAP<sup>22,23</sup>. All 10 individuals had colorectal polyposis,  
100 with between 16 and >100 colonic adenomas, six were known to have duodenal polyps, five had  
101 colorectal cancer and one developed jejunal and pancreatic neuroendocrine cancer (Extended Data  
102 Table 1).

103  
104 **Mutation rates in normal intestinal stem cells**

105 An intestinal crypt is constituted predominantly of a population of epithelial cells arising from a single  
106 recent common ancestor<sup>34-36</sup>. The somatic mutations which have accumulated over the course of the  
107 individual's lifetime in the ancestral crypt stem cell are present in all its descendant cells<sup>3</sup>. Thus, by  
108 sequencing individual crypts, somatic mutations present in the ancestral stem cell can be identified.  
109 Using laser-capture microdissection, 144 individual normal intestinal crypts (large intestine n=107 and  
110 small intestine n=37) were isolated from the 10 individuals with germline *MUTYH* mutations (Extended  
111 Data Table 2). DNA libraries were prepared from individual crypts using a bespoke low-input DNA  
112 library preparation method<sup>37</sup> and were whole-genome sequenced at a mean 28-fold coverage.  
113

114 The single base substitution (SBS) mutation burdens of individual crypts ranged from a median for  
115 each individual of 2,294 to 33,350, equating to mutation rates of 79-1470 SBS/year, 2-33-fold higher  
116 than normal crypts from wild-type individuals (~43 SBS/year)<sup>3</sup> (Figure 1b). Therefore, all normal crypts  
117 from all MAP individuals studied showed elevated somatic mutation rates (Figure 1a-b).  
118

119 Differences in mutation rate were observed between individuals with MAP (Figure 1b). A 33-fold  
120 higher rate of SBS accumulation than in wild-type crypts<sup>3</sup> was observed in PD44890, a 16 year old male  
121 with *MUTYH*<sup>Y179C+/- G396D+/-</sup>. By contrast, the nine other individuals showed only 2- to 5-fold increases in  
122 mutation rate compared to wild type. The reason for this substantial difference is not clear. However,  
123 in addition to the *MUTYH* mutations, PD44890 carried two heterozygous germline missense variants  
124 in *OGG1* (Extended Data Figure 1), one of which (R46Q) is reported to impair *OGG1* activity in  
125 experimental systems<sup>38,39</sup> and has been observed as somatically mutated in human cancer<sup>40</sup>. Germline  
126 *OGG1* mutations are not currently recognised as causing cancer predisposition in humans<sup>41</sup>. However,  
127 if either or both of these mutations results in defective 8-OG excision they could account for the  
128 substantially elevated mutation rate in PD44890, particularly in the context of defective *MUTYH*  
129 activity.  
130

131 There was also evidence of differences in mutation rates between the various *MUTYH* germline  
132 genotypes studied (Fig. 1b). Excluding the outlier individual PD44890, mutation rates were lower in  
133 individuals with the compound heterozygous *MUTYH*<sup>Y179C+/- G396D+/-</sup> (102 SBS/year, range 61-182) than  
134 individuals with *MUTYH*<sup>Y179C+/-</sup> (214 SBS/year, range 84-356), *MUTYH*<sup>Y104\*+/-</sup> (204 SBS/year, range 153-  
135 309) or *MUTYH*<sup>G286E+/-</sup> (152 SBS/year, range 82-238) (*MUTYH*<sup>Y179C+/- G396D+/-</sup> vs *MUTYH*<sup>Y179C+/-</sup> /  
136 *MUTYH*<sup>Y104\*+/-</sup> / *MUTYH*<sup>G286E+/-</sup>,  $P=9.5\times10^{-8}$ ,  $P=6.1\times10^{-19}$ ,  $P=9.8\times10^{-3}$  respectively. *MUTYH*<sup>G286E+/-</sup> vs.  
137 *MUTYH*<sup>Y179C+/-</sup> / *MUTYH*<sup>Y104\*+/-</sup>  $P=2.7\times10^{-2}$  and  $P=4.5\times10^{-3}$  respectively). The results, therefore, indicate  
138 that different *MUTYH* genotypes confer differentially elevated mutation rates and that the extent of  
139 the mutation rate increase can be modified by other factors.  
140

141 SBS mutation rates in coding exons in normal intestinal crypts from MAP individuals were also  
142 elevated compared to wild-type individuals (Extended Data Fig 2a-b). These increases were, however,  
143 slightly smaller than those observed in the genome-wide mutation rate (Extended Data Fig 2a-b).  
144 Nonsense, missense and synonymous mutation rates were all increased compared with wild-type  
145 crypts, with the greatest increase observed in nonsense mutations (~10-fold more nonsense than  
146 wild-type vs ~3.5-fold more missense and ~2.6-fold more synonymous) (Extended Data Fig. 2c). This  
147 is attributable to the mutational signatures present (see below) and the tendency of specific mutations  
148 at particular trinucleotide contexts to preferentially generate protein-truncating mutations<sup>42,43</sup>.  
149

150 Neoplastic glands from 13 intestinal adenomas from five individuals with MAP showed SBS mutation  
151 burdens that were, on average, ~2-fold higher (range 1.2 to 2.5 fold) (Figure 1c) than normal crypts  
152 from the same individuals sampled at the same time. Therefore, the elevated mutation rate observed  
153 in histologically normal intestinal crypts in individuals with germline *MUTYH* mutations is further  
154 increased during the process of neoplastic transformation, as previously observed in wild type  
155 individuals<sup>44,45</sup>.

156

157 Small insertion and deletion (ID) mutations accumulated at a rate of 2.1 ID/yr (linear mixed-effects  
158 model, 95% confidence interval (C.I.) 1.2-3.0,  $P = <10^{-4}$ ), which is higher than in wild-type controls (1.3  
159 ID/yr, linear mixed-effects model, C.I. 0.54-2.0,  $P = 0.0011$ )<sup>3,43</sup>. The cause of this modestly elevated ID  
160 rate is not clear. In two MAP individuals additional mutational processes could explain the higher  
161 burdens observed in these cases. In PD44890 the high ID mutation rate (ID rate 6/yr) was, at least  
162 partially, explained by the presence of an additional ID generating mutational process associated with  
163 exposure to the mutagen colibactin produced by a strain of *E.Coli*<sup>3,46,47</sup> present in the colonic  
164 microbiome of some people (see below). In PD50747 (ID rate 6/yr), a previously undescribed sporadic  
165 ID signature IDA was identified which was not present in other MAP individuals (described below).  
166 Structural rearrangements and copy number changes were only observed in a small number of normal  
167 intestinal crypts, at similar frequencies to those in wild-type controls (Extended Data Table 2)<sup>3</sup>.  
168

169

### **Mutational signatures**

170 Mutational signatures were extracted from the combined catalogues of SBS mutations from all normal  
171 and neoplastic intestinal crypts and glands using two independent methods. We then decomposed  
172 each *de novo* extracted signature into known COSMIC reference mutational signatures. Finally, we  
173 used these decompositions to estimate the contribution of each reference signature to each sample  
174 (Methods, Supplementary Note). Three *de novo* extracted signatures, N1-N3, accounted for the  
175 majority of mutations, all of which were mainly characterised by C>A mutations (Fig. 2a). Two of these  
176 closely corresponded to the reference mutational signatures SBS18 and SBS36. The third was  
177 abundant only in individual PD44890 (the individual with a high mutation rate carrying *OGG1* germline  
178 variants) (Fig. 2b and Supplementary Note) but could also be accounted for by a combination of SBS18  
179 and SBS36 according to the standard parameters used for decomposition (Supplementary  
180 Information).

181

182 Following decomposition and signature attribution, four reference SBS mutational signatures, SBS1,  
183 SBS5, SBS18 and SBS36 were identified in all samples (Fig. 3, Supplementary Note). SBS1, due to  
184 deamination of 5-methylcytosine at CG dinucleotides and SBS5, of unknown aetiology, have both been  
185 found ubiquitously in normal and cancer cells and accumulate in a more or less linear fashion with  
186 age<sup>2-4,8,33,48-50</sup>. SBS18, thought to result from DNA damage due to reactive oxygen species, has  
187 previously been reported in normal colorectal cells<sup>3</sup> and many types of cancer<sup>33</sup> and is characterised  
188 by C>A mutations predominantly at ACA, CCA, GCA and TCT trinucleotide contexts (mutated base  
189 underlined) (Fig. 2a and Fig. 3). SBS36 has previously been found in cancers with germline or somatic  
190 *MUTYH* mutations and is also characterised by C>A mutations, albeit with a different profile of  
191 preferred trinucleotide contexts from SBS18<sup>30-33</sup> (Fig. 2a). SBS88, which is predominantly characterised  
192 by T>C and T>G mutations, and is due to early life exposure to the mutagenic agent colibactin  
193 produced by some strains of *E.Coli*<sup>3,46,47</sup>, was observed in a subset of crypts from PD44890 (Figure 3b).

194 The SBS88 mutation burdens were consistent with those previously seen in wild type individuals  
195 indicating that MUTYH is unlikely to be implicated in the genesis of SBS88.

196

197 The increased SBS mutation burdens in normal crypts from individuals with *MUTYH* germline  
198 mutations appeared to be due to the contributions of SBS18 and SBS36 mutations (Fig. 3a-e). The  
199 proportions of SBS18 and SBS36, however, differed between *MUTYH* germline genotypes. SBS18  
200 accounted for a substantially higher proportion of mutations in crypts and glands from individuals  
201 with the *MUTYH*<sup>Y179C+/- G396D+/-</sup> genotype (n=85 crypts) than in individuals with the *MUTYH*<sup>Y179C+/-</sup>,  
202 *MUTYH*<sup>Y104\*+/-</sup> and *MUTYH*<sup>G286E+/-</sup> genotypes (n=59 crypts, Extended Data Fig. 3a). Since *MUTYH*<sup>Y104\*</sup>  
203 causes *MUTYH* protein truncation, it is conceivable that SBS36 is the consequence of complete loss of  
204 *MUTYH* function and therefore that this is also effected by *MUTYH*<sup>Y179C</sup> and *MUTYH*<sup>G286E</sup>. Conversely,  
205 *MUTYH*<sup>G396D</sup> may retain partial activity<sup>14,21</sup> and thus generates a signature more closely resembling  
206 SBS18 which is found in normal tissues with fully active *MUTYH*.

207

208 The *de novo* extracted mutational signature N2, which primarily contributes to the mutational spectra  
209 of crypts from PD44890 (*MUTYH*<sup>Y179C+/- G396D+/-</sup>), resembled reference signature SBS18  
210 (<https://cancer.sanger.ac.uk/cosmic/signatures>) but showed differences, notably with over  
211 representation of C>A mutations at GCA and, to a lesser extent, CCA and ACA trinucleotides (mutated  
212 base underlined) (Fig. 2a-b and Extended Data Fig. 1). A signature reported in human cells with *in vitro*  
213 engineered biallelic *OGG1* deletion is also primarily characterised by C>A mutations at GCA and ACA  
214 trinucleotides<sup>51</sup>. It is, therefore, possible that mutagenesis due to the germline *OGG1* variant(s) in  
215 PD44890 (see above) is superimposed on the mutational signature produced by the *MUTYH* germline  
216 mutations to generate N2 (see Supplementary Information for further analysis and discussion).

217

218 The mutational signatures in adenoma glands were similar to those seen in normal crypts from the  
219 same individuals (Fig. 3a,b,d,e). SBS36 and SBS18 were principally responsible for the increased  
220 mutation burdens observed in adenomas compared to normal crypts.

221

222 Candidate cancer “driver” mutations, defined as known or likely oncogenic hotspot mutations and  
223 truncating mutations in tumour suppressor genes (Methods), were observed in 15% of normal crypts  
224 (22/144), more than double the rate observed in wild-type crypts from comparable healthy controls;  
225 6% (25/449)<sup>3,43</sup>. A substantial proportion of candidate drivers (16/22) were nonsense mutations,  
226 mirroring the broader exome-wide increase in nonsense mutations (Extended Data Fig. 2c), and  
227 reflecting the proclivity of certain mutation types to generate truncating mutations<sup>29,42,43</sup>. The  
228 mutational spectrum of driver mutations in normal crypts and neoplastic glands resembled the  
229 genome-wide spectra with substantial contributions from SBS18 and SBS36 (Extended Data Fig. 4).  
230 Hence, the mutational processes resulting from defective *MUTYH* activity appear to promote the  
231 accumulation of putative cancer driver mutations in normal and neoplastic tissues<sup>52,53</sup>.

232

233 Three known ID signatures were identified. ID1 & ID2 are characterised predominantly by insertions  
234 and deletions of single T bases at T mononucleotide repeats which are associated with strand slippage  
235 during DNA replication and are seen in most human cancers and normal tissues<sup>1-4,8,33</sup>. ID18 is  
236 associated with colibactin exposure, is found in normal intestinal stem cells and certain cancers, and  
237 usually associated with SBS88<sup>3,47</sup>. ID1 was the dominant signature in normal cells whereas ID2  
238 predominated in neoplastic cells (Extended Data Fig. 5). ID18 was principally observed in samples from

239 PD44890 and is responsible for the elevated ID rate in this individual (Extended Data Fig. 6). A further  
240 ID signature, IDA, identified in PD50747, was characterised by single C insertions at C mononucleotide  
241 repeats (Extended Data Fig. 6). IDA was present in both normal crypts (~5% of total ID burden) and to  
242 a greater extent in adenoma glands (~20% of total ID burden). The cause of this previously undescribed  
243 signature is unclear but may be associated with previous capecitabine treatment and seems unlikely  
244 to be related to germline *MUTYH* mutations.

245

#### 246 **Mutations in other cell types**

247 To investigate whether the elevated mutation rates and mutational signatures observed in intestinal  
248 epithelium caused by defective *MUTYH* are present in other cell types, peripheral white blood cell and  
249 tissue lymphocyte DNAs from individuals with biallelic *MUTYH* mutations were whole genome  
250 sequenced using a duplex sequencing method (NanoSeq)<sup>50</sup> that allows mutation calling from single  
251 DNA molecules and thus accurately discovers somatic mutations in tissues in which multiple clonal  
252 lineages are intimately mixed.

253

254 The white blood cell SBS mutation rates of all individuals with *MUTYH* mutations were higher than  
255 wild-type controls ( $n=15$  granulocyte samples from 9 healthy individuals aged 20-80yrs)(Fig. 4)(25  
256 SBS/yr vs 19 SBS/yr, linear mixed-effects model,  $R^2=0.89$ , *MUTYH*; 95% C.I., 19-31,  $P=10^{-7}$  and wild-  
257 type; 95% C.I., 14-24,  $P=10^{-6}$ ). The relative increases in blood mutation rates were lower than in  
258 intestinal crypts from each individual (Fig. 4b). Nevertheless, the relative increases paralleled the  
259 differential increases observed between individuals in intestinal crypts. SBS mutation rates in tissue  
260 lymphocytes were modestly raised compared with wild-type healthy individuals (Fig. 4d) (53 SBS/yr  
261 vs 40 SBS/yr, linear mixed-effects model,  $R^2=0.68$ , *MUTYH*; 95% C.I., 21-85,  $P=0.01$  and wild-type; 95%  
262 C.I., 13-66,  $P=0.01$ ). The signatures associated with defective *MUTYH*, SBS18 and SBS36, contributed  
263 the excess mutations in all samples (Fig. 4c and Fig. 4e). An additional mutational signature was seen  
264 in lymphocytes. SBS9, which is associated with DNA polymerase eta mediated somatic hypermutation  
265 and is a key process in the physiological maturation of B-cells, was observed in most lymphocyte  
266 samples indicating that the lymphocyte cell populations contained mature B-cells (Fig. 4e).

267

#### 268 **DISCUSSION**

269 This study shows elevated base substitution somatic mutation rates due to SBS18 and/or SBS36 in  
270 normal tissues from individuals with *MUTYH* mutations. The results are compatible with all intestinal,  
271 and potentially all other cells in the body, showing elevated mutation rates. The relative increases in  
272 mutation rate and mutational signature composition differed between individuals, probably due to  
273 different *MUTYH* mutations and perhaps to other modifying influences.

274

275 We have previously highlighted the capability of normal human cells to tolerate substantially elevated  
276 mutation rates<sup>43</sup>. Carriers of POLE and POLD1 germline exonuclease domain mutations exhibited  
277 elevated somatic mutation burdens without evident cellular or organismal consequences, other than  
278 an increased cancer risk<sup>43</sup>. This capability is confirmed in *MUTYH* germline mutation carriers. It is  
279 further emphasised by the observation of a 33-fold genome-wide elevated base substitution mutation  
280 burden in the 16 year old PD44890, which would confer a “mutational age” of ~500 years, without  
281 overt evidence of premature ageing. The increase in mutation burden in coding exons is lower than  
282 genome-wide in POLE/POLD1 mutation carriers. Similarly, in individuals with *MUTYH* mutations there  
283 is a smaller increase of coding exon than genome-wide mutation burdens (Extended Data Fig. 2a-b).

284 Nevertheless in PD44890 the increase is still ~29-fold, and therefore equivalent to a “mutational age”  
285 of ~450 years. Whilst lesser increases in mutation rates compared to wild-type individuals were  
286 observed in other tissues from PD44890, ~8-fold in white blood cells and ~7 fold in tissue lymphocytes,  
287 these still conferred substantially elevated “mutational ages” in the absence of features of premature  
288 ageing. Thus direct deleterious effects of base substitutions accumulated over the course of a lifetime  
289 may not be an important cause of ageing.

290

291 The elevated mutation rate in normal intestinal epithelium likely contributes to the increased risk of  
292 colorectal adenomas and cancers in individuals with *MUTYH* mutations. Indeed, there appears to be  
293 a correlation between the extent of elevation of mutation rate and the rate of acquisition of colorectal  
294 adenomas. Individuals with the *MUTYH*<sup>Y104\*+/+</sup> and *MUTYH*<sup>Y179C+/+</sup> genotypes exhibited greater  
295 increases in somatic mutation rates than individuals with the *MUTYH*<sup>Y179C+/- G396D+/-</sup> genotype. Previous  
296 detailed clinical phenotyping of large series indicates that individuals with biallelic truncating  
297 mutations or *MUTYH*<sup>Y179C+/+</sup> show higher rates of accumulation of adenomas and earlier age of onset  
298 of carcinoma<sup>22,23</sup> than *MUTYH*<sup>Y179C+/- G396D+/-</sup>. The correlation between elevation of mutation rate and  
299 severity of clinical phenotype is further highlighted by individual PD44890 (16 years of age,  
300 *MUTYH*<sup>Y179C+/- G396D+/-</sup>) who exhibited a substantially higher mutation rate than others of this genotype,  
301 and showed a much accelerated rate of colorectal adenoma development (Extended Data Table 1-2).  
302 We previously described ~7-fold elevated genome-wide base substitution mutation rates in intestinal  
303 cells of POLE germline exonuclease domain mutation carriers<sup>43</sup>. POLE mutation carriers, however,  
304 show lower colorectal adenoma rates than *MUTYH* biallelic mutation carriers who generally only show  
305 2-5 fold increased mutation rates. This apparent discrepancy may, however, be explained by the  
306 genomic distribution of mutations. In POLE mutation carriers there is relative sparing of coding  
307 sequences, with only a three to four fold increase in exonic mutations in intestinal cells, whereas this  
308 sparing is less pronounced in *MUTYH* mutation carriers leading to similar increases in exonic mutation  
309 rates (Extended Data Fig. 7a-b). These observations lead to the proposition that measurements of  
310 somatic coding mutation rates undertaken early in life could, in future, be used to refine individual  
311 cancer risk predictions for *POLE/POLD* and *MUTYH* germline mutation carriers.

312

313 As for many other cancer predisposition syndromes, it is unclear why *MUTYH* germline mutations lead  
314 particularly to intestinal neoplasia. Elevated somatic mutation rates are also found in white blood cells  
315 in MAP individuals (and may therefore be present in other tissues) although the increases appear  
316 lesser in extent than in intestinal cells. The propensity to generate SBS18 mutations appears greater  
317 in wild type intestinal cells than in other cell types<sup>49</sup> and this may also be contributory.

318

319 In summary, we report elevated somatic base substitution rates characterised by distinctive  
320 mutational signatures in normal tissues from individuals with MAP. These findings underscore  
321 previous observations that elevated somatic base substitution rates are largely tolerated by cells and  
322 do not overtly accelerate the process of ageing. It is likely, however, that increased mutation rates in  
323 normal intestinal cells throughout life lead to increased rates of accumulation of driver mutations and,  
324 hence, the procession of neoplastic clones culminating in cancer.

325

326

327

328

329  
330  
331  
332  
333  
334  
335  
336  
337  
338  
339  
340  
341  
342  
343  
344  
345  
346  
347  
348  
349  
350

351 **REFERENCES**

352

353 1 Yoshida, K. *et al.* Tobacco smoking and somatic mutations in human bronchial epithelium. *Nature* **578**,  
354 266-272, doi:10.1038/s41586-020-1961-1 (2020).

355 2 Moore, L. *et al.* The mutational landscape of normal human endometrial epithelium. *Nature* **580**, 640-  
356 646, doi:10.1038/s41586-020-2214-z (2020).

357 3 Lee-Six, H. *et al.* The landscape of somatic mutation in normal colorectal epithelial cells. *Nature* **574**,  
358 532-537, doi:10.1038/s41586-019-1672-7 (2019).

359 4 Brunner, S. F. *et al.* Somatic mutations and clonal dynamics in healthy and cirrhotic human liver.  
360 *Nature* **574**, 538-542, doi:10.1038/s41586-019-1670-9 (2019).

361 5 Martincorena, I. *et al.* Somatic mutant clones colonize the human esophagus with age. *917*, 911-917  
362 (2018).

363 6 Martincorena, I., Jones, P. H. & Campbell, P. J. Constrained positive selection on cancer mutations in  
364 normal skin. *Proceedings of the National Academy of Sciences* **113**, E1128-E1129,  
365 doi:10.1073/pnas.1600910113 (2016).

366 7 Blokzijl, F. *et al.* Tissue-specific mutation accumulation in human adult stem cells during life. *Nature*  
367 **538**, 260-264, doi:10.1038/nature19768 (2016).

368 8 Lawson, A. R. J. *et al.* Extensive heterogeneity in somatic mutation and selection in the human  
369 bladder. *Science* **370**, 75-82, doi:10.1126/science.aba8347 (2020).

370 9 Balaban, R. S., Nemoto, S. & Finkel, T. Mitochondria, oxidants, and aging. *Cell* **120**, 483-495,  
371 doi:10.1016/j.cell.2005.02.001 (2005).

372 10 Cooke, M. S., Evans, M. D., Dizdaroglu, M. & Lunec, J. Oxidative DNA damage: mechanisms, mutation,  
373 and disease. *FASEB J* **17**, 1195-1214, doi:10.1096/fj.02-0752rev (2003).

374 11 Cheng, K. C., Cahill, D. S., Kasai, H., Nishimura, S. & Loeb, L. A. 8-Hydroxyguanine, an Abundant Form  
375 of Oxidative DNA Damage, Causes G -> T and a -> C Substitutions. *Journal of Biological Chemistry* **267**,  
376 166-172 (1992).

377 12 Rosenquist, T. A., Zharkov, D. O. & Grollman, A. P. Cloning and characterization of a mammalian 8-  
378 oxoguanine DNA glycosylase. *Proceedings of the National Academy of Sciences of the United States of  
379 America* **94**, 7429-7434, doi:DOI 10.1073/pnas.94.14.7429 (1997).

380 13 McGoldrick, J. P., Yeh, Y. C., Solomon, M., Essigmann, J. M. & Lu, A. L. Characterization of a  
381 Mammalian Homolog of the Escherichia-Coli MutY Mismatch Repair Protein. *Molecular and Cellular  
382 Biology* **15**, 989-996 (1995).

383 14 Komine, K. *et al.* Functional Complementation Assay for 47 MUTYH Variants in a MutY-Disrupted  
384 Escherichia coli Strain. *Hum Mutat* **36**, 704-711, doi:10.1002/humu.22794 (2015).

385 15 Ruggieri, V. *et al.* Loss of MUTYH function in human cells leads to accumulation of oxidative damage  
386 and genetic instability. *Oncogene* **32**, 4500-4508, doi:10.1038/onc.2012.479 (2013).

387 16 Wooden, S. H., Bassett, H. M., Wood, T. G. & McCullough, A. K. Identification of critical residues  
388 required for the mutation avoidance function of human MutY (hMYH) and implications in colorectal  
389 cancer. *Cancer Letters* **205**, 89-95, doi:10.1016/j.canlet.2003.10.006 (2004).

390 17 Kundu, S., Brinkmeyer, M. K., Livingston, A. L. & David, S. S. Adenine removal activity and bacterial  
391 complementation with the human MutY homologue (MUTYH) and Y165C, G382D, P391L and Q324R  
392 variants associated with colorectal cancer. *DNA Repair* **8**, 1400-1410,  
393 doi:10.1016/j.dnarep.2009.09.009 (2009).

394 18 Parker, A. R. *et al.* Cells with pathogenic biallelic mutations in the human MUTYH gene are defective  
395 in DNA damage binding and repair. *Carcinogenesis* **26**, 2010-2018, doi:10.1093/carcin/bgi166 (2005).

396 19 Sampson, J. R., Jones, S., Dolwani, S. & Cheadle, J. P. MutYH (MYH) and colorectal cancer. *Biochem Soc  
397 Trans* **33**, 679-683, doi:10.1042/BST0330679 (2005).

398 20 Sampson, J. R. *et al.* Autosomal recessive colorectal adenomatous polyposis due to inherited  
399 mutations of MYH. *Lancet* **362**, 39-41, doi:10.1016/S0140-6736(03)13805-6 (2003).

400 21 Al-Tassan, N. *et al.* Inherited variants of MYH associated with somatic G : C -> T : A mutations in  
401 colorectal tumors. *Nature Genetics* **30**, 227-232, doi:10.1038/ng828 (2002).

402 22 Collaborative Group on Duodenal Polyposis in, M. A. P. *et al.* Duodenal Adenomas and Cancer in  
403 MUTYH-associated Polyposis: An International Cohort Study. *Gastroenterology* **160**, 952-954 e954,  
404 doi:10.1053/j.gastro.2020.10.038 (2021).

405 23 Nielsen, M. *et al.* Analysis of MUTYH genotypes and colorectal phenotypes in patients With MUTYH-  
406 associated polyposis. *Gastroenterology* **136**, 471-476, doi:10.1053/j.gastro.2008.10.056 (2009).

407 24 Lubbe, S. J., Di Bernardo, M. C., Chandler, I. P. & Houlston, R. S. Clinical implications of the colorectal  
408 cancer risk associated with MUTYH mutation. *J Clin Oncol* **27**, 3975-3980,  
409 doi:10.1200/JCO.2008.21.6853 (2009).

410 25 Win, A. K. *et al.* Risk of colorectal cancer for carriers of mutations in MUTYH, with and without a  
411 family history of cancer. *Gastroenterology* **146**, 1208-1211 e1201-1205,  
412 doi:10.1053/j.gastro.2014.01.022 (2014).

413 26 Theodoratou, E. *et al.* A large-scale meta-analysis to refine colorectal cancer risk estimates associated  
414 with MUTYH variants. *Br J Cancer* **103**, 1875-1884, doi:10.1038/sj.bjc.6605966 (2010).

415 27 Cleary, S. P. *et al.* Germline MutY human homologue mutations and colorectal cancer: a multisite  
416 case-control study. *Gastroenterology* **136**, 1251-1260, doi:10.1053/j.gastro.2008.12.050 (2009).

417 28 Vogt, S. *et al.* Expanded extracolonic tumor spectrum in MUTYH-associated polyposis.  
418 *Gastroenterology* **137**, 1976-1985 e1971-1910, doi:10.1053/j.gastro.2009.08.052 (2009).

419 29 Thomas, L. E. *et al.* Burden and profile of somatic mutation in duodenal adenomas from patients with  
420 familial adenomatous- and MUTYH-associated polyposis. *Clinical Cancer Research* **23**, 6721-6732,  
421 doi:10.1158/1078-0432.CCR-17-1269 (2017).

422 30 Rashid, M. *et al.* Adenoma development in familial adenomatous polyposis and MUTYH -associated  
423 polyposis: Somatic landscape and driver genes. *Journal of Pathology* **238**, 98-108,  
424 doi:10.1002/path.4643 (2016).

425 31 Viel, A. *et al.* A Specific Mutational Signature Associated with DNA 8-Oxoguanine Persistence in  
426 MUTYH-defective Colorectal Cancer. *EBioMedicine* **20**, 39-49, doi:10.1016/j.ebiom.2017.04.022  
427 (2017).

428 32 Pilati, C. *et al.* Mutational signature analysis identifies MUTYH deficiency in colorectal cancers and  
429 adrenocortical carcinomas. *J Pathol* **242**, 10-15, doi:10.1002/path.4880 (2017).

430 33 Alexandrov, L. B. *et al.* The repertoire of mutational signatures in human cancer. *Nature* **578**, 94-101,  
431 doi:10.1038/s41586-020-1943-3 (2020).

432 34 Ritsma, L. *et al.* Intestinal crypt homeostasis revealed at single-stem-cell level by in vivo live imaging.  
433 *Nature* **507**, 362-365, doi:10.1038/nature12972 (2014).

434 35 Snippert, H. J. *et al.* Intestinal Crypt Homeostasis Results from Neutral Competition between  
435 Symmetrically Dividing Lgr5 Stem Cells. *Cell* **143**, 134-144, doi:10.1016/j.cell.2010.09.016 (2010).

436 36 Barker, N. *et al.* Identification of stem cells in small intestine and colon by marker gene Lgr5. *Nature*  
437 **449**, 1003-1007, doi:10.1038/nature06196 (2007).

438 37 Ellis, P. *et al.* Reliable detection of somatic mutations in solid tissues by laser-capture microdissection  
439 and low-input DNA sequencing. *Nat Protoc*, doi:10.1038/s41596-020-00437-6 (2020).

440 38 Audebert, M. *et al.* Alterations of the DNA repair gene OGG1 in human clear cell carcinomas of the  
441 kidney. *Cancer Res* **60**, 4740-4744 (2000).

442 39 Audebert, M., Radicella, J. P. & Dizdaroglu, M. Effect of single mutations in the OGG1 gene found in  
443 human tumors on the substrate specificity of the Ogg1 protein. *Nucleic Acids Res* **28**, 2672-2678,  
444 doi:10.1093/nar/28.14.2672 (2000).

445 40 Forbes, S. A. *et al.* COSMIC: Somatic cancer genetics at high-resolution. *Nucleic Acids Research* **45**,  
446 D777-D783, doi:10.1093/nar/gkw1121 (2017).

447 41 Mur, P. *et al.* Germline variation in the oxidative DNA repair genes NUDT1 and OGG1 is not associated  
448 with hereditary colorectal cancer or polyposis. *Hum Mutat* **39**, 1214-1225, doi:10.1002/humu.23564  
449 (2018).

450 42 Temko, D. *et al.* Somatic POLE exonuclease domain mutations are early events in sporadic  
451 endometrial and colorectal carcinogenesis , determining driver mutational landscape , clonal  
452 neoantigen burden and immune response. 283-296, doi:10.1002/path.5081 (2018).

453 43 Robinson, P. S. *et al.* Elevated somatic mutation burdens in normal human cells due to defective DNA  
454 polymerases. *bioRxiv* (2020).

455 44 Lin, S. H. *et al.* The somatic mutation landscape of premalignant colorectal adenoma. *Gut* **67**, 1299-  
456 1305, doi:10.1136/gutjnl-2016-313573 (2018).

457 45 Roerink, S. F. *et al.* Intra-tumour diversification in colorectal cancer at the single-cell level. *Nature* **556**,  
458 457-+, doi:10.1038/s41586-018-0024-3 (2018).

459 46 Pleguezuelos-Manzano, C. *et al.* Mutational signature in colorectal cancer caused by genotoxic  
460 pks(+)E. coli. *Nature* **580**, 269-+, doi:10.1038/s41586-020-2080-8 (2020).

461 47 Olafsson, S. *et al.* Somatic Evolution in Non-neoplastic IBD-Affected Colon. *Cell* **182**, 672-684 e611,  
462 doi:10.1016/j.cell.2020.06.036 (2020).

463 48 Alexandrov, L. B. *et al.* Clock-like mutational processes in human somatic cells. *Nature Genetics* **47**,  
464 1402-1407, doi:10.1038/ng.3441 (2015).

465 49 Moore, L. *et al.* The mutational landscape of human somatic and germline cells. *bioRxiv* (2020).

466 50 Abascal, F. *et al.* Somatic mutation landscapes at single-molecule resolution. *Nature*,  
467 doi:10.1038/s41586-021-03477-4 (2021).

468 51 Zou, X. Q. *et al.* A systematic CRISPR screen defines mutational mechanisms underpinning signatures  
469 caused by replication errors and endogenous DNA damage. *Nature Cancer*, doi:10.1038/s43018-021-  
470 00200-0 (2021).

471 52 Xie, Y. *et al.* Deficiencies in mouse Myh and Ogg1 result in tumor predisposition and G to T mutations  
472 in codon 12 of the K-ras oncogene in lung tumors. *Cancer Res* **64**, 3096-3102, doi:10.1158/0008-  
473 5472.can-03-3834 (2004).

474 53 Jones, S. *et al.* Increased frequency of the k-ras G12C mutation in MYH polyposis colorectal  
475 adenomas. *Br J Cancer* **90**, 1591-1593, doi:10.1038/sj.bjc.6601747 (2004).

476 54 Jones, D. *et al.* cgpCaVEManWrapper: Simple Execution of CaVEMan in Order to Detect Somatic Single  
477 Nucleotide Variants in NGS Data. *Curr Protoc Bioinformatics* **56**, 15 10 11-15 10 18,  
478 doi:10.1002/cpbi.20 (2016).

479 55 Coorens, T. H. H. *et al.* Embryonal precursors of Wilms tumor. *Science* **366**, 1247-+,  
480 doi:10.1126/science.aax1323 (2019).

481 56 Nik-Zainal, S. *et al.* Mutational processes molding the genomes of 21 breast cancers. *Cell* **149**, 979-  
482 993, doi:10.1016/j.cell.2012.04.024 (2012).

483 57 Raine, K. M. *et al.* cgPindel: Identifying Somatically Acquired Insertion and Deletion Events from  
484 Paired End Sequencing. *Curr Protoc Bioinformatics* **52**, 15 17 11-15 17 12,  
485 doi:10.1002/0471250953.bi1507s52 (2015).

486 58 Van Loo, P. *et al.* Allele-specific copy number analysis of tumors. *Proc Natl Acad Sci U S A* **107**, 16910-  
487 16915, doi:10.1073/pnas.1009843107 (2010).

488 59 Raine, K. M. *et al.* ascatNgs: Identifying Somatically Acquired Copy-Number Alterations from Whole-  
489 Genome Sequencing Data. *Curr Protoc Bioinformatics* **56**, 15 19 11-15 19 17, doi:10.1002/cpbi.17  
490 (2016).

491 60 Teh, Y. W., Jordan, M. I., Beal, M. J. & Blei, D. M. Hierarchical Dirichlet processes. *Journal of the  
492 American Statistical Association* **101**, 1566-1581, doi:10.1198/016214506000000302 (2006).

493 61 Gori, K. & Baez-Ortega, A. sigfit: flexible Bayesian inference of mutational signatures. *bioRxiv* (2020).

494 62 Martincorena, I. *et al.* Universal Patterns of Selection in Cancer and Somatic Tissues. *Cell* **171**, 1029-  
495 1041 e1021, doi:10.1016/j.cell.2017.09.042 (2017).

496 63 Sondka, Z. *et al.* The COSMIC Cancer Gene Census: describing genetic dysfunction across all human  
497 cancers. *Nat Rev Cancer* **18**, 696-705, doi:10.1038/s41568-018-0060-1 (2018).

498

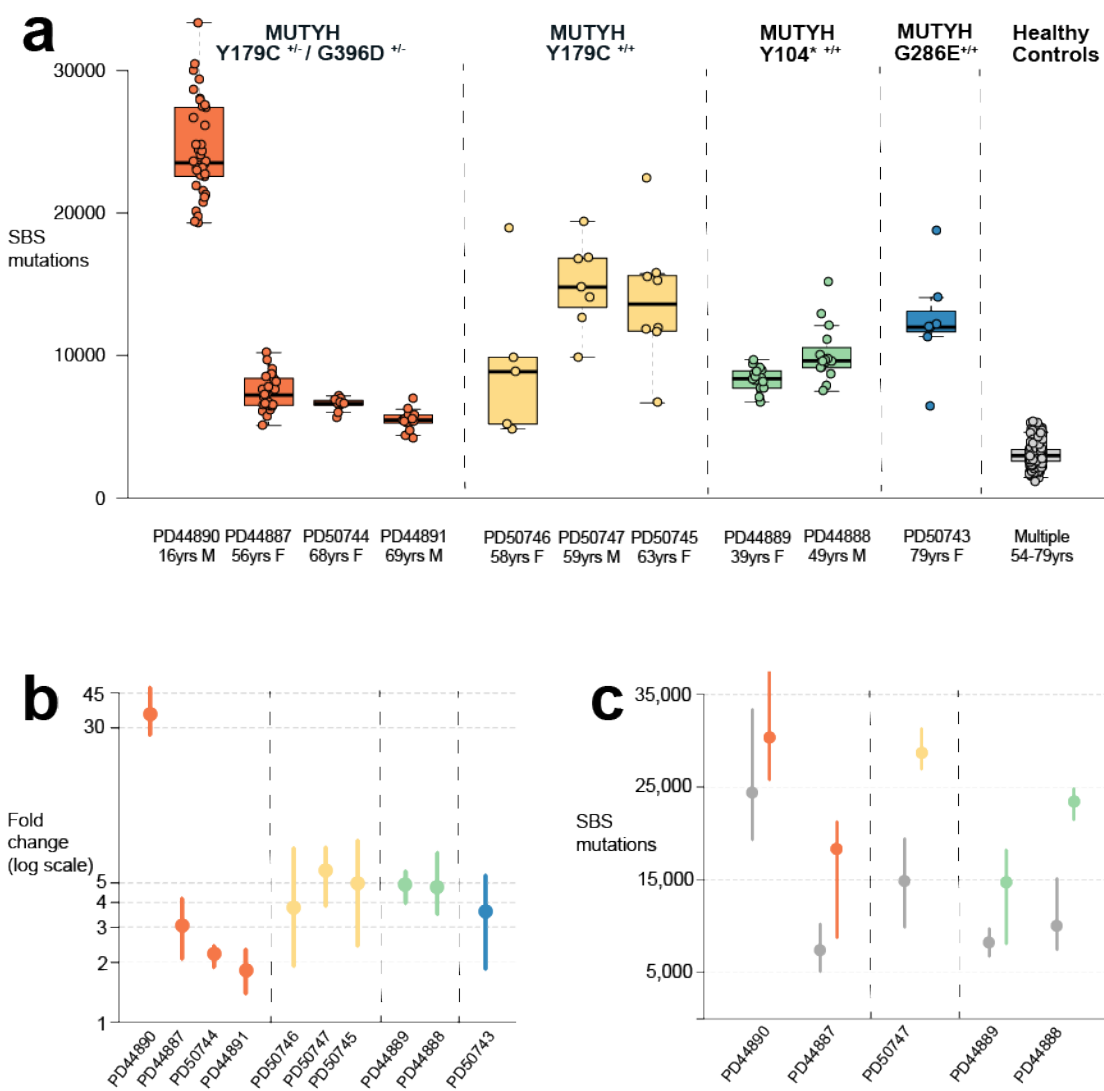
499

500

501

502

503 **FIGURES**  
504



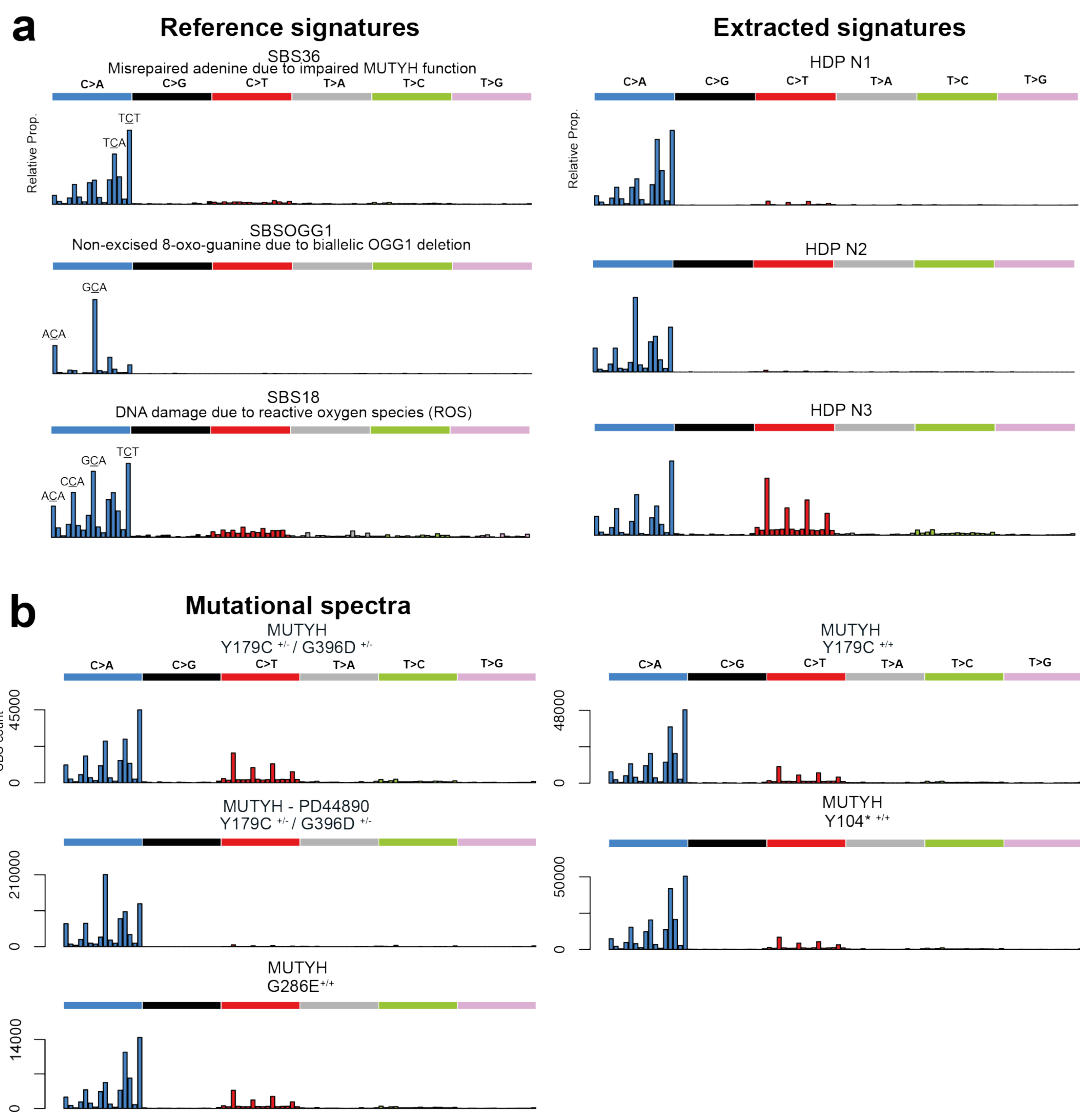
505

506

507 **FIGURE 1 | Somatic mutation burdens in cells with MUTYH mutations**

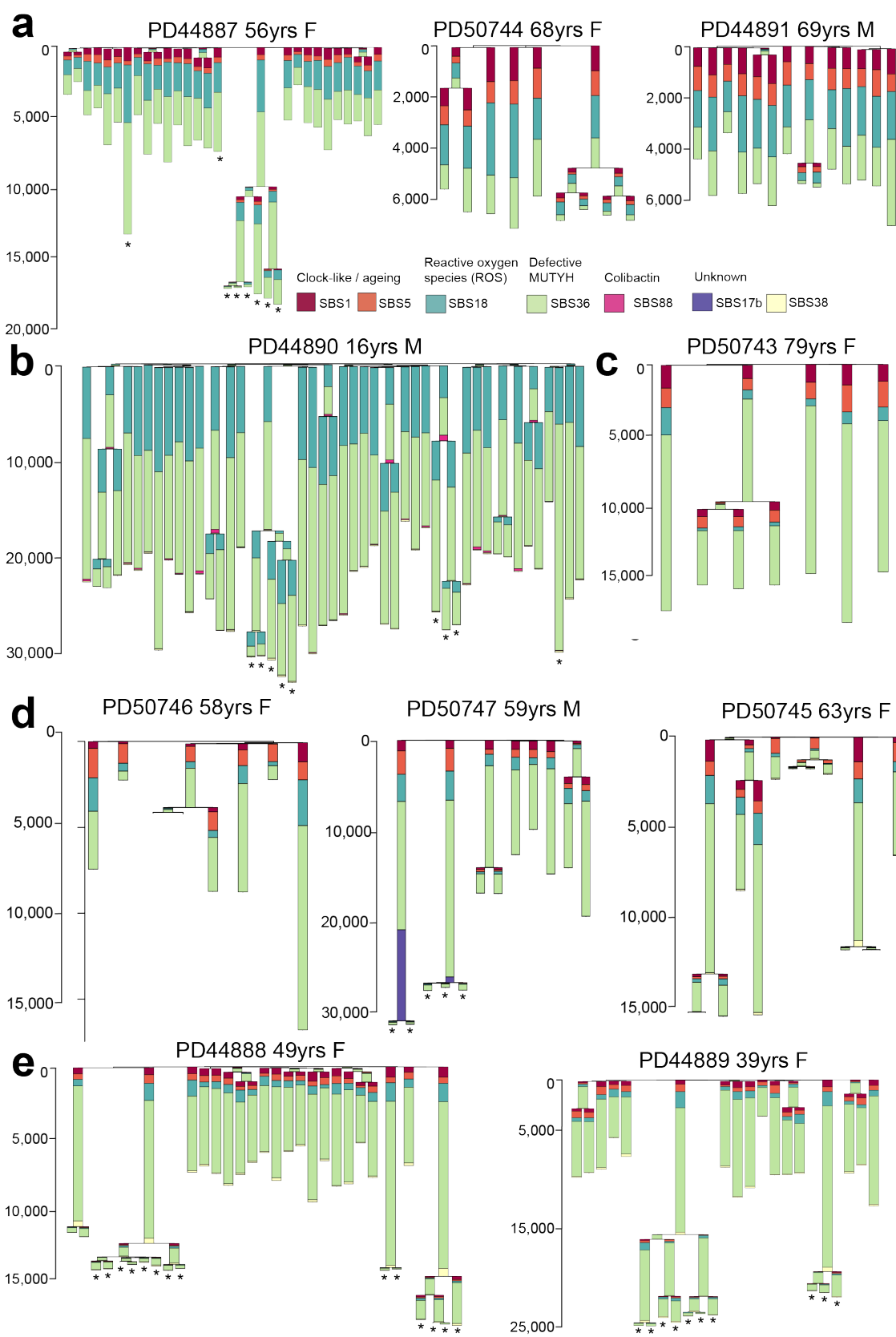
508 Elevated mutation burdens in normal intestinal cells with *MUTYH* mutations (a) Genome-wide single  
509 base substitution (SBS) mutation burden of individual intestinal crypts grouped according to patient.  
510 Each dot represents an individual intestinal crypt. *MUTYH* genotypes are displayed separately.  
511 Boxplots display median, inter-quartile range (IQR) from 1<sup>st</sup> to 3<sup>rd</sup> quartiles and whiskers extend from  
512 the last quartile to the last data point that is within 1.5x IQR (b) Fold-change in SBS rate compared  
513 with wild-type controls<sup>3</sup> coloured according to germline genotype (orange; *MUTYH*<sup>Y179C+/- G396D+/-</sup>,  
514 yellow; *MUTYH*<sup>Y179C+/+</sup>, green; *MUTYH*<sup>Y104\*+/+</sup>, blue; *MUTYH*<sup>G286E+/+</sup>). Median values are represented by  
515 the dot, whiskers represent the range from the minimum to maximum value. P-values for pair-wise  
516 comparisons are shown in Supplementary Note. (c) Genome-wide single base substitution burden in  
517 histologically normal crypts (grey) and adenoma crypts (orange, yellow and green) arranged by patient

518 and germline mutation. Median values represented by the dot, whiskers represent the range from the  
519 minimum to maximum value. Data available for 5 individuals who had adenoma crypts sequenced.  
520



521  
522  
523  
524  
525  
526  
527  
528  
529  
530

**FIGURE 2 | Mutational spectra and signature components from normal cells with MUTYH mutations**  
**(a)** Probability distribution for COSMIC reference signature SBS36<sup>40</sup>, recently described OGG1 deletion signature SBSOGG1<sup>51</sup> and reference signature SBS18<sup>40</sup>. Mutational signature components N1-3 from HDP *de novo* signature extraction (see Supplementary Information for all components and Methods / Supplementary Note for further explanation). **(b)** Mutational spectra in normal tissues displayed by the germline MUTYH mutation. Distinctive peaks are annotated with their trinucleotide context (mutated base is underlined). PD44890 is displayed separately to highlight the difference in spectrum observed in this individual.

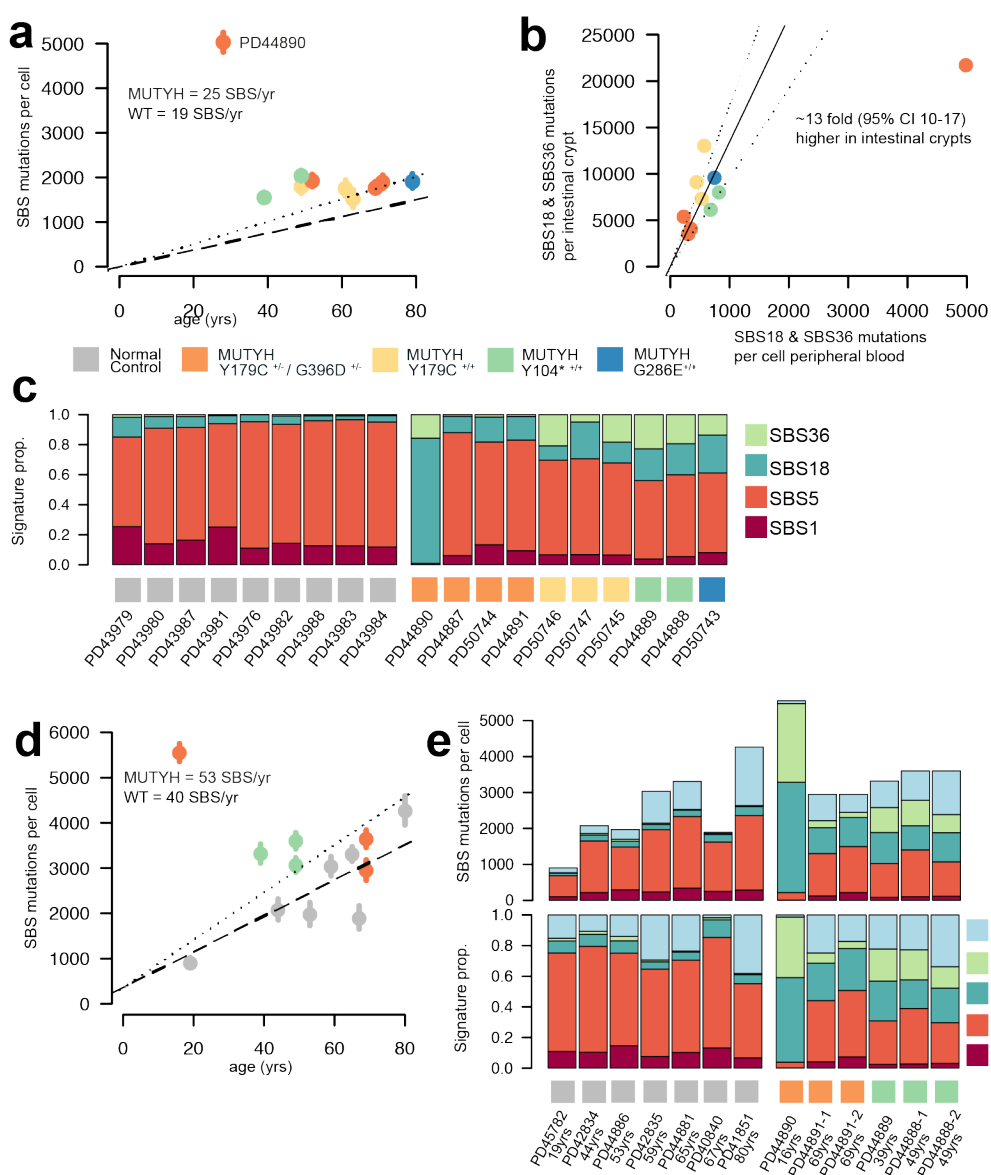


531  
532  
533  
534

**FIGURE 3 | Phylogenetic trees and mutational signatures intestinal cells with germline *MUTYH* mutations**

535 Phylogenetic trees per-individual reconstructed from SBS mutations in individual intestinal crypts  
536 showing the number of SBS mutations per branch. Stacked barplots are overlaid onto each branch to  
537 represent the proportion of each mutational signature contributing to that branch. Phylogenetic trees  
538 are arranged by *MUTYH* germline mutation; (a) *MUTYH*<sup>Y179C+/- G396D+/-</sup> (b) *MUTYH*<sup>Y179C+/- G396D+/-</sup> with  
539 OGG1 germline mutations, (c) *MUTYH*<sup>G286E+/-</sup>, (d) *MUTYH*<sup>Y179C+/-</sup> and (e) *MUTYH*<sup>Y104\*+/-</sup>. Adenoma glands  
540 bearing cancer driver mutations are indicated with an asterisk \*\*.  
541

542



543

544 **FIGURE 4 | Mutation burdens and mutational signatures in blood and immune cell populations**

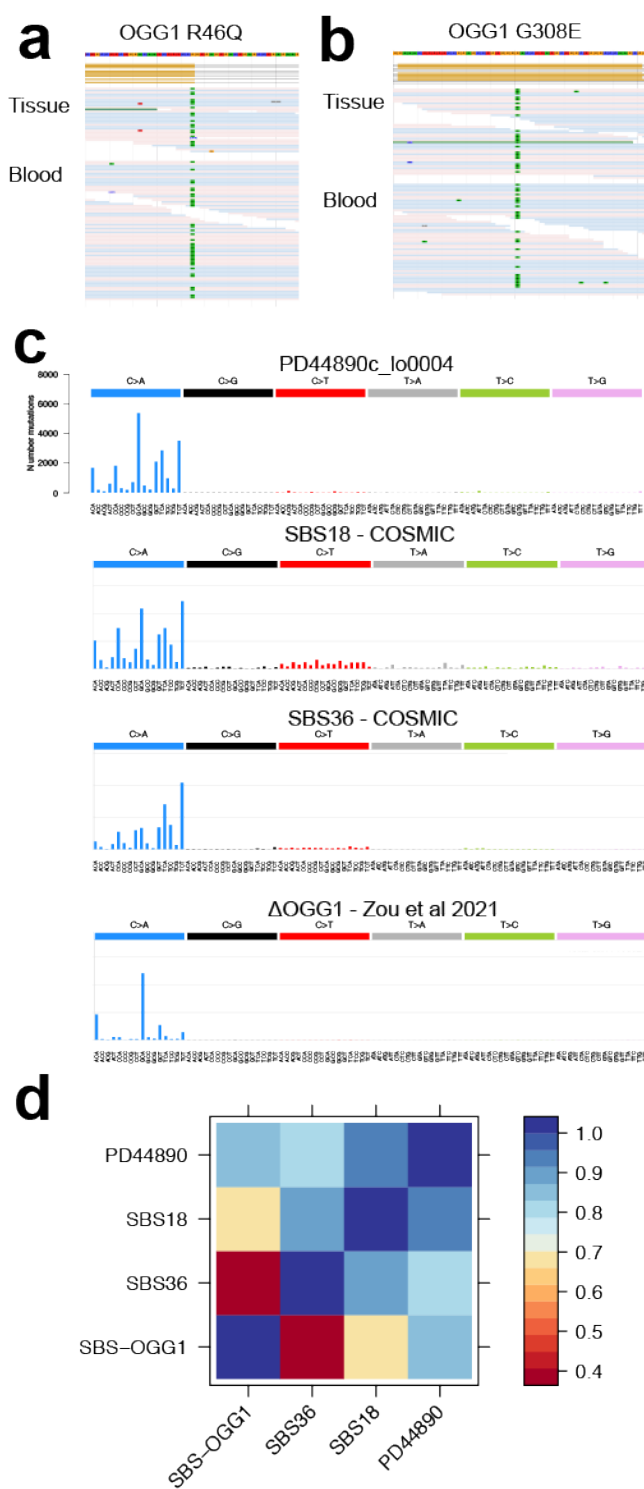
545 **(a)** Mutation burden in peripheral blood. SBS mutation burden per cell plotted against the age of the  
 546 individual in years coloured according to the individual's germline mutation; orange; MUTYH<sup>Y179C+/-</sup>  
 547 G396D+/-, yellow; MUTYH<sup>Y179C+/-</sup>, green; MUTYH<sup>Y104\*+/-</sup> and blue; MUTYH<sup>G286E+/-</sup>. Whiskers represent the  
 548 95% confidence interval. Black dashed line represents the average mutation rate in normal wild-type  
 549 control samples<sup>50</sup> **(b)** Mutation burden of MUTYH associated mutational signatures; SBS18 and SBS36  
 550 per cell for peripheral blood (x-axis) against the SBS18 & SBS36 mutation burden of normal intestinal  
 551 crypts (y-axis). Each dot represents one individual and they are coloured according to the individual's  
 552 germline mutation; orange; MUTYH<sup>Y179C+/- G396D+/-</sup>, yellow; MUTYH<sup>Y179C+/-</sup>, green; MUTYH<sup>Y104\*+/-</sup> and  
 553 blue; MUTYH<sup>G286E+/-</sup>. Ratio MUTYH mutational processes in colon vs blood ~13x fold (linear model, 95%  
 554 C.I.; 10-17). Black line indicates ratio and dotted lines the 95% confidence intervals. **(c)** Stacked bar  
 555 plot displaying the mutational signature contribution in each peripheral blood sample organised by  
 556 patient. Coloured squares indicate the MUTYH germline mutation. Normal control data from

557 granulocytes sequenced using the same method (data from Abascal et al 2021)<sup>50</sup>. Significantly higher  
558 proportion of SBS18 and SBS36 are observed in individuals with *MUTYH* mutations vs normal healthy  
559 controls (two-sided Wilcoxon rank sum,  $P=0.00004$ ) **(d)** SBS mutation burden in intestinal lymphocyte  
560 cells from wild-type healthy individuals (grey) and individuals with *MUTYH* mutations (coloured  
561 according to the germline *MUTYH* genotype) plotted against age (years). Dots represent median  
562 values and whiskers represent the 95% confidence interval. Dashed line indicates the rate of increase  
563 of SBS burden in wild-type lymphocytes (40 SBS/yr, linear mixed-effects model,  $R^2=0.68$ , 95% C.I., 13-  
564 66,  $P=0.01$ ) and dotted line indicates the rate of increase in SBS burden in lymphocytes from  
565 individuals with *MUTYH* mutations (53 SBS/yr, linear mixed-effects model,  $R^2=0.68$ , 95% C.I., 21-85,  
566  $P=0.01$ ). **(e)** Stacked bar plots showing the absolute (above) and relative (below) contributions of each  
567 mutational signature in tissue lymphocytes from wild-type healthy individuals (grey squares) and  
568 individuals with *MUTYH* mutations (coloured squares).

569

570

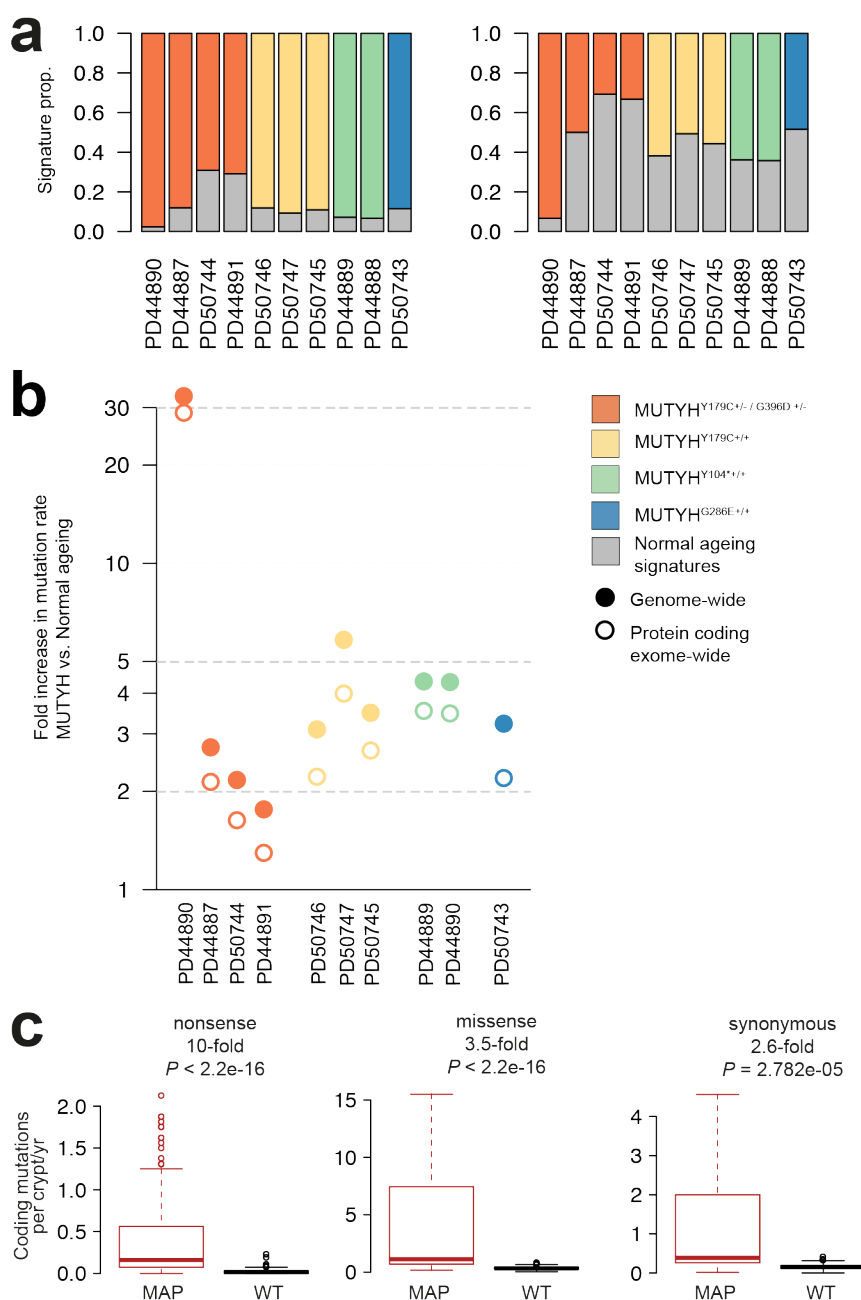
571 EXTENDED FIGURES



573 **Extended Data Figure 1 | Germline mutations and mutational spectrum of somatic mutations in**  
574 **PD44890**

575 Two candidate germline modifier mutations were identified in individual PD44890 both of which are  
576 in the oxoguanine glycosylase (OGG1) gene which is a key component of the base excision repair  
577 pathway and a partner of MUTYH in the repair of 8-oxo-guanine DNA lesions. Both mutations are  
578 heterozygous nonsynonymous mutations. JBrowse images are displayed showing the reads for each  
579 mutation; **(a)** OGG1 R46Q **(b)** OGG1 R308E. See Supplementary Note for further discussion of these  
580 putative germline modifier mutations. **(c)** Mutational spectrum of SBS mutations from a  
581 representative intestinal crypt from individual PD44890, mutational spectra for the COSMIC reference  
582 signatures SBS36 and SBS18 are displayed below for comparison ( <https://cancer.sanger.ac.uk/cosmic/signatures>). Mutational spectrum of IPS cells with homozygous  
583 OGG1 deletion (Zou et al 2021, Nature Cancer)<sup>51</sup> denoted SBS OGG1. **(d)** Matrix displaying cosine  
584 similarity between the observed spectrum in individual PD44890 and reference signatures SSB18,  
585 SBS36 and SBS OGG1.

587



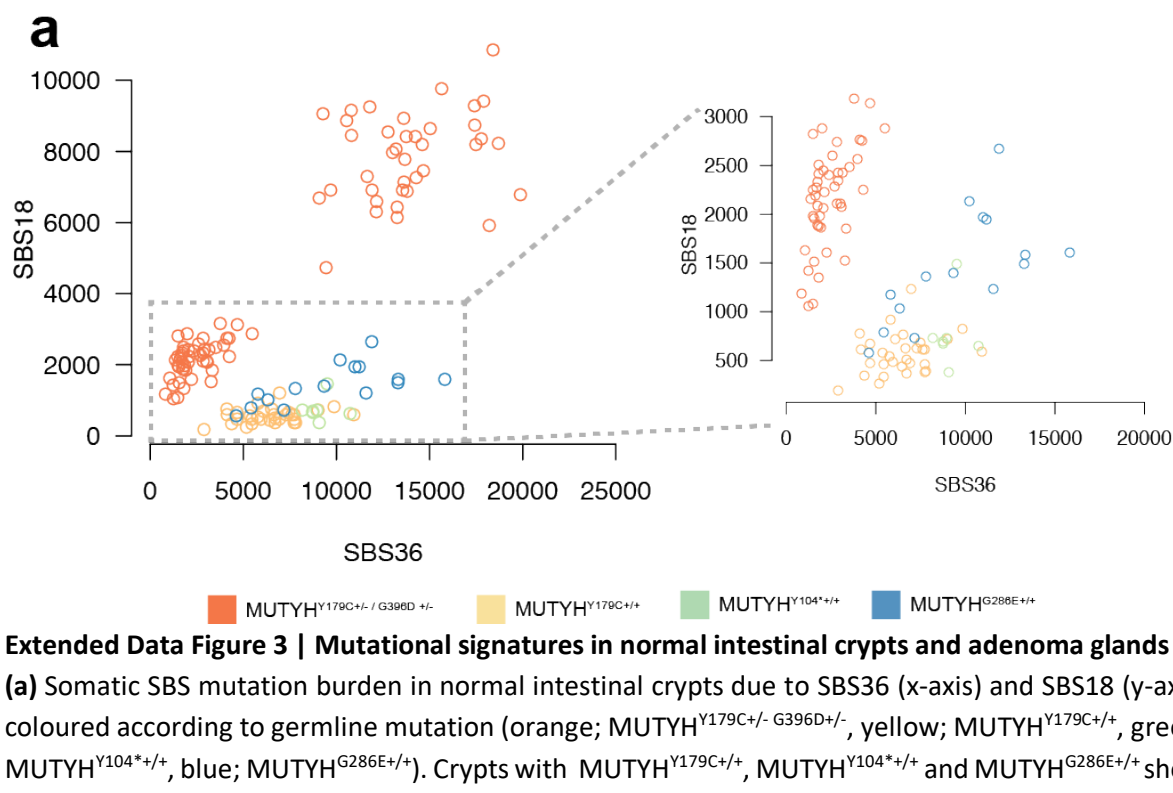
588  
589  
590  
591  
592  
593  
594  
595  
596  
597  
598  
599

### Extended Data Figure 2 | Genome-wide and exome-wide mutation burdens in intestinal crypts

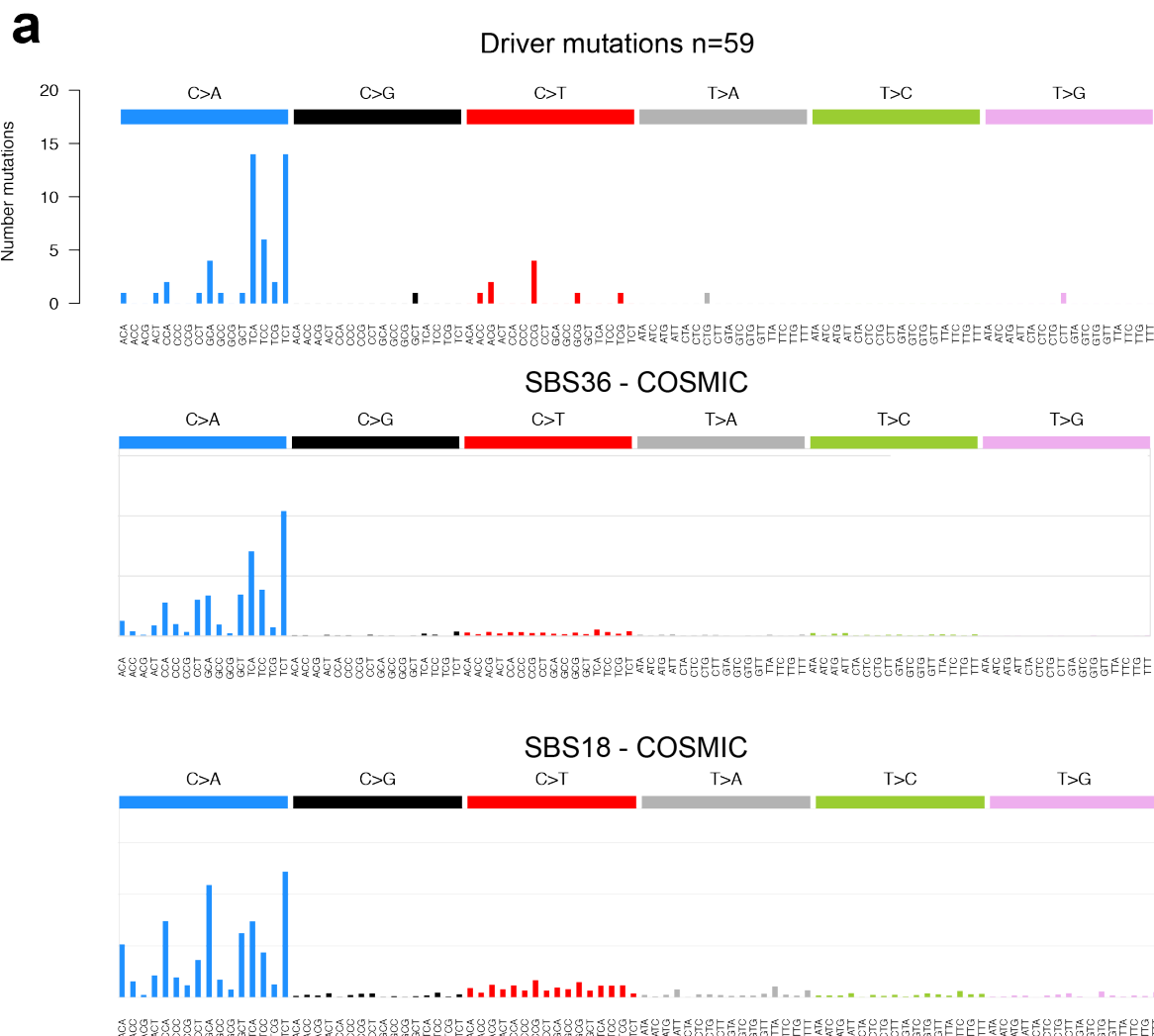
(a) Stacked bar plots show the proportion of SBS mutations contributed by MUTYH-related signatures SBS18 and SBS36 (coloured bar) and normal ageing signatures (SBS1 and SBS5) (grey bar). Genome-wide signature proportions (left) protein-coding exome-wide signature proportions (right). (b) Fold-increase in the genome- and exome-wide mutation burden of samples from individuals with MUTYH-Associated Polyposis (MAP) compared with normal controls plotted on a logarithmic scale. (c) Boxplots showing nonsense, missense and synonymous coding mutation rates (SBS mutations/crypt/year) in histologically normal intestinal crypts from individuals with MUTYH-Associated Polyposis (MAP) (red) and healthy individuals; wild type (WT) (black). Boxplots display median, inter-quartile range (IQR) from 1<sup>st</sup> to 3<sup>rd</sup> quartiles and whiskers extend from the last quartile to the last data point that is within 1.5x IQR. Fold changes compared to WT, are shown above each

600 pair, *P*-values calculated using a two-sided Wilcoxon test. Data for healthy wild-type individuals from  
601 Lee-Six et al 2019<sup>3</sup>  
602

603



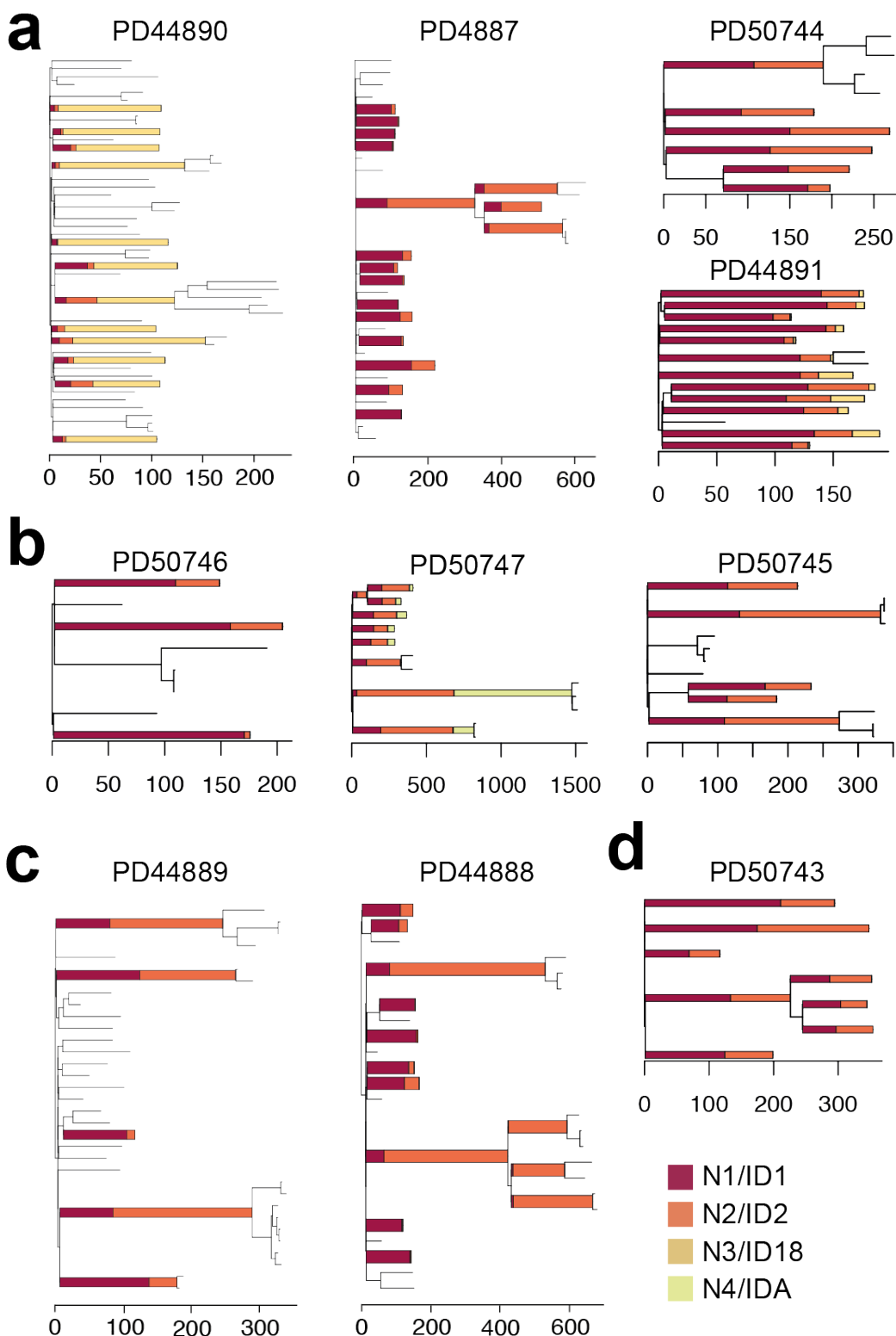
613  
614



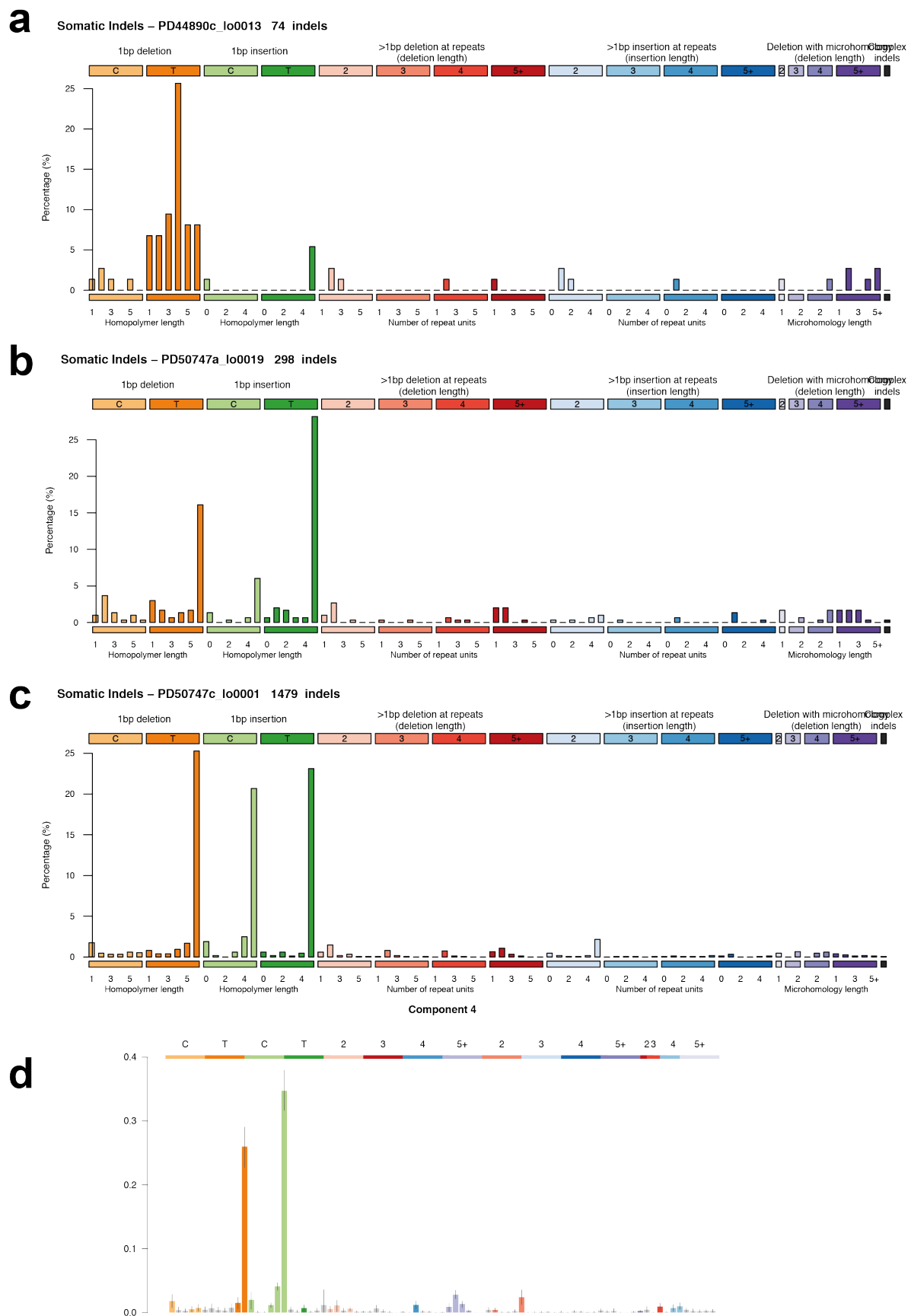
615  
616 **Extended Data Figure 4 | Mutational Spectrum of driver mutations in normal and neoplastic**  
617 **intestinal crypts**

618 **(a)** Mutational spectrum of drivers mutations identified in normal and neoplastic intestinal stem cells  
619 in this cohort (n=59). Mutational spectra for the COSMIC reference signatures **(b)** SBS36 and **(c)** SBS18  
620 are displayed below for comparison. The spectra of driver mutations is dominated by SBS36 and  
621 SBS18. COSMIC reference signatures available at: <https://cancer.sanger.ac.uk/cosmic/signatures>.

622  
623



625 **Extended Data Fig 5 | Phylogenetic trees showing ID signature exposure**  
626 Phylogenetic trees with ID signature exposure overlaid. Branches of the phylogenetic tree with >100  
627 somatic ID mutations have been converted into stacked bar plots displaying the contribution of each  
628 HDP signature component / mutational process to that branch: N1/ID1 shown in dark red, N2/ID2 in  
629 orange, N3/ID18 in mustard yellow and N4/IDA in lime green. Phylogenetic trees organised by  
630 germline genotype, **(a)** MUTYH<sup>Y179C+/- G396D+/-</sup>, **(b)** MUTYH<sup>Y179C+/-</sup>, **(c)** MUTYH<sup>Y104\*+/-</sup> and **(d)** MUTYH<sup>G286E+/-</sup>  
631  
632



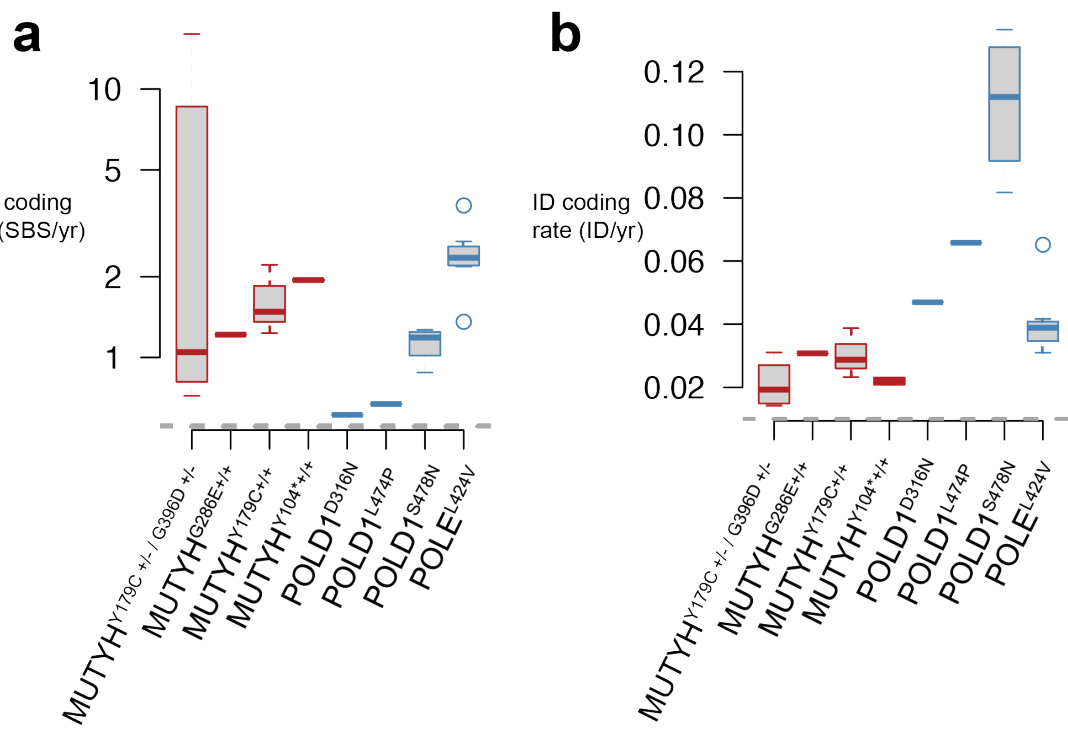
633

634

### Extended Data Figure 6 | ID mutational spectra

635 ID mutational spectra for crypts with sporadic ID signature exposures. (a) Representative sample from  
 636 PD44890 with high ID18 exposure. Representative normal crypt from PD50747 showing IDA exposure

637 in **(b)** normal crypt and **(c)** adenoma gland. **(d)** ID signature component arising from unconditioned *de*  
638 *novo* HDP signature extraction (Methods) corresponding to signature IDA.  
639  
640



641  
642 **Extended Data Figure 7 | Coding mutation burdens in intestinal crypts from individuals with**  
643 **germline MUTYH and POLE/D1 mutations**  
644 Coding mutation burdens in individuals with *MUTYH* and *POLE/D1*. (a) SBS coding mutation rate  
645 (SBS/year) coloured according to cohort; *MUTYH*; red, *POLE/D1*; blue. (b) ID coding mutation rate  
646 (ID/year).  
647

648

649 **Extended Data Table 1 | Clinical summary and phenotypic characteristics of individuals with**  
**650 germline *MUTYH* mutations**

651 Summary of phenotypic features and disease burden in all individuals in this cohort.

652

653 **Extended Data Table 2 | Summary of samples sequenced including germline *MUTYH* mutation,**  
**654 sequencing method and mutation burdens**

655

656 **Extended Data Table 3 | Cancer driver mutations identified in this cohort**

657 Cancer driver mutations identified across all samples in this cohort

658

659

660 **METHODS**

661

662 **Ethical approval and study participants**

663 This research complies with all relevant ethical regulations. MAP patients were recruited as part of Wales  
664 Research Ethics Committee (REC) 12-WA0071 and 15-WA0075 and samples collected were approved for use in  
665 this project by REC 18/ES/0133. Normal healthy controls were recruited as part of the following UK Research  
666 Ethics Committee (REC) studies; 15/WA/0131, 15/EE/0152, 18/ES/0133 and 08/h0304/85+5.

667

668 Informed consent was obtained from all participants and no monetary compensation was offered for their  
669 participation. A complete list of study participants and tissue samples is summarised in Extended Data Table 1  
670 and 2.

671

672 **DNA extraction from bulk samples**

673 Frozen whole blood underwent DNA extraction using the Gentra Puregene Blood Kit (Qiagen). Briefly, 1-2ml of  
674 frozen blood were thawed, lysed in RBC lysis solution and centrifuged. Cell pellet was resuspended in cell lysis  
675 solution and incubated at 37 °C for 2 hours. RNA and protein was degraded using RNase A solution and protein  
676 precipitation solution. DNA was precipitated with isopropanol.

677

678 **Tissue Preparation**

679 Tissues were embedded in Optimal Cutting Temperature (OCT) compound, frozen histological sections were cut  
680 at 25-30µm and mounted on polyethylene naphthalate (PEN) slides and fixed in 70% ethanol for 5 minutes  
681 followed by two washes with phosphate buffered saline for 1 minute each. Slides were manually stained in  
682 haematoxylin and eosin using a conventional staining protocol. A subset of samples were fixed in RNAlater  
683 (Sigma Aldrich) according to manufacturer's instructions. Fixed tissue samples were embedded in paraffin using  
684 a Tissue-Tek tissue processing machine (Sakura). No formalin was used in the preparation, storage, fixation or  
685 processing of samples. Processed tissue blocks were embedded in paraffin wax, sectioned to 10µm thickness  
686 and mounted onto PEN slides (Leica). Tissue slides were stained using a standard haematoxylin and eosin (H&E)  
687 protocol. Slides were temporarily cover-slipped and scanned on a NanoZoomer S60 Slide Scanner (Hamamatsu),  
688 images were viewed with NDP.View2 software (Hamamatsu).

689

690 **Laser Capture Microdissection**

691 Laser capture microdissection was undertaken using a LMD7000 microscope (Leica) into a skirted 96-well PCR  
692 plate. Cell lysis was undertaken using 20µl proteinase-K PicoPure® DNA Extraction kit (Arcturus®), samples  
693 were incubated at 65 °C for 3 hours followed by proteinase denaturation at 75 °C for 30 minutes. Thereafter  
694 samples were stored at -20 °C prior to DNA library preparation.

695

696 **Low-input DNA library preparation and sequencing**

697 DNA library preparation of micro-dissected tissue samples was undertaken as previously described using a  
698 bespoke low-input enzymatic-fragmentation-based library preparation method<sup>2-4,37</sup>. This method was employed  
699 as it allows for high quality DNA library preparation from very low starting quantity of material (from 100-500  
700 cells). DNA library concentration was assessed after library preparation and used to guide choice of samples to  
701 take forward to DNA sequencing, minimum library concentration was 5ng/µL and libraries with >15ng/µL were  
702 preferentially chosen. 150bp paired-end Illumina reads were prepared with Unique Dual Index barcodes  
703 (Illumina).

704

705 DNA sequencing was undertaken on a NovaSeq 6000 platform using an XP kit (Illumina). Samples were  
706 multiplexed in pools of 6-24 samples. Pools were sequenced to achieve a coverage of ~30x.

707

708 **Mutation calling and post-processing filters**

709 Sequencing reads were aligned to NCBI human genome GRCh37 and aligned using the Burrow-Wheeler  
710 Alignment (BWA-MEM). Single Base Substitutions (SBS) were called using the 'Cancer Variants through  
711 Expectation Maximization' algorithm (CaVEMan)<sup>54</sup>. Mutations were called using an unmatched normal synthetic  
712 bam file to retain early embryonic and somatic mutations. Post-processing filters were applied to remove low-  
713 input library preparation specific artefacts and germline mutations using a previously described method<sup>1,2,37,55</sup>.  
714 Filters applied were: (1) common single nucleotide polymorphisms were removed by filtering against a panel of  
715 75 unmatched normal samples<sup>56</sup> (2) to remove mapping artefacts, mutations were required to have a minimum  
716 median read alignment score of mutant reads (ASMD  $\geq$  140) and fewer than half of the reads supporting the  
717 mutation should be clipped (CLPM =0); (3) a filter to remove overlapping reads that result from the relatively  
718 short insert size which could lead to double counting of variant reads; and (4) a filter to remove cruciform DNA  
719 structures that can arise during the low-input library preparation method.  
720

721 Next, we applied multiple filters to remove germline variants and potential artefacts whilst retaining *bona fide*  
722 embryonic and somatic variants. This approach has been detailed in previous publications and the code for these  
723 filters can be found at [https://github.com/TimCoorens/Unmatched\\_NormSeq](https://github.com/TimCoorens/Unmatched_NormSeq). Mutations were aggregated per  
724 patient and a read pile-up was performed using an in-house algorithm (cgpVAF) to tabulate the read count of  
725 mutant and reference reads per sample for each mutation locus. Germline mutations were filtered out using an  
726 exact binomial test. The exact binomial test is used to distinguish germline from somatic variants and uses the  
727 aggregate read counts from all samples of the same patient<sup>1,55</sup>. In brief, the read depth across all samples from  
728 that individual was calculated (median in this study 496-fold). This high coverage yields a very precise estimate  
729 of the true VAF of each mutation. While the VAF estimates of the earliest embryonic SNVs and germline variants  
730 from samples sequenced at 30x might overlap, the VAFs from the aggregate coverage from that individual will  
731 be distinguishable using statistical testing. To achieve this, the beta-binomial test was applied. The  
732 overdispersion parameter (rho) threshold for genuine variants of rho>0.1 was used.  
733

734 Phylogenetic trees were created using MPBoot (version 1.1.0 bootstrapped - 1000) and mutations were mapped  
735 to branches using maximum likelihood assignment.  
736

737 Indels (ID) were called using Pindel<sup>57</sup> using the same synthetic unmatched normal sample employed in SBS  
738 mutation calling. ID calls were filtered to remove calls with a quality score of <300 ('Qual'; sum of mapping  
739 qualities of the supporting reads) and a read depth of less than 15. Thereafter, ID filtering was performed in a  
740 similar manner as SBS to remove germline variants and library preparation / sequencing artefacts.  
741

#### 742 **Copy-number alteration calling**

743 Somatic copy-number variants (CNVs) were called using the Allele-Specific Copy number Analysis of Tumours  
744 (ASCAT) algorithm<sup>58</sup>, <https://github.com/Crick-CancerGenomics/ascat> in the ascatNGS package<sup>59</sup>. Bulk blood  
745 samples or phylogenetically unrelated normal samples were used as matched normals. ASCAT was initially run  
746 with default parameters. To reduce the number of false-positive calls that arise when analysing normal tissue  
747 samples using ASCAT, a bespoke algorithm ascat-PCA was applied. ascat-PCA extracts a noise profile by  
748 aggregating the LogR ratio from across a panel of normal unrelated samples and subtracts this signature from  
749 that observed in the sample being analysed using principal component analysis (INSERT GITHUB).  
750

#### 751 **Structural variant calling**

752 Whole-genome sequences were analysed for somatic structural variants (SVs) using the Genomic  
753 Rearrangement Identification Software Suite (GRIDSS). In preparation for this analysis, genomes were remapped  
754 to Human Genome Version 38 and GRIDSS was run using the same matched normal as used for CNV analysis.  
755 Coordinates for SV calls were subsequently converted back to GRCh37. SV calls in L1 transposon donor regions  
756 and fragile sites were excluded from the final SV analysis.  
757

758 **Mutational signature analysis**  
759 The R package HDP (<https://github.com/nicolaroberts/hdp>), based on the hierarchical Dirichlet process<sup>60</sup>, was  
760 used to extract mutational signatures. Analysis of mutational signatures using this package has been applied to  
761 normal tissues previously<sup>1-4</sup>. In brief, this nonparametric Bayesian method models categorical count data using  
762 the hierarchical Dirichlet process. A hierarchical structure is established using patients as the first tier (parent  
763 nodes) and individual samples as the second tier (dependent nodes). Uniform Dirichlet priors were applied  
764 across all samples. The algorithm creates a mutation catalogue for each sample and infers the distribution of  
765 signatures in any one sample using a Gibbs sampler. We performed mutational signatures analysis per-branch,  
766 counting each branch of the phylogenetic tree as a distinct sample to avoid double counting of mutations. Since  
767 the MCMC process scales linearly with the number of counts, we randomly subsampled each branch to a  
768 maximum of 2500 total substitutions. Branches with fewer than 100 mutations were excluded from the  
769 mutational signature extraction. No reference signatures were included as priors.  
770

771 To assess the contribution of each mutational process, mutational signatures were refitted to all mutation  
772 counts of branches of phylogenies using the R package sigfit (<https://github.com/kgori/sigfit>)<sup>61</sup>. To avoid  
773 overfitting, a limited subset of reference mutational signatures were included per patient corresponding to the  
774 HDP signatures that have been identified in that individual.  
775

776 Ageing signatures SBS1 and SBS5 are present in all normal intestinal crypts<sup>3</sup>. Lower than expected burdens of  
777 SBS1 and SBS5 were observed in most individuals in this study due to; 1. the inherent challenges of accurately  
778 estimating mutation burden in hypermutated samples and 2. the appreciable contamination of reference  
779 signatures with SBS1 and SBS5. To partially address this, we used the extracted HDP component corresponding  
780 to SBS36 in the refitting stage which has lower SBS1 and SBS5 contamination than the COSMIC reference SBS36  
781 signature. Nevertheless, in individual PD44890 where SBS18 and SBS36 exposures are many tens of times  
782 greater than the normal mutation rate, the estimates of SBS1 and SBS5 are substantially lower than would be  
783 expected.  
784  
785  
786

787 **Cancer driver mutations**  
788 Cancer driver mutations were identified using two methods aiming to identify genes and mutations in this cohort  
789 that are subject to positive selection. Firstly, to identify mutations in cancer genes under positive selection in an  
790 unbiased manner, we ran a modified dNdS method<sup>62</sup>. To avoid double-counting of mutations, only unique  
791 mutations (SBS and ID) which were mapped to branches of the phylogenetic trees were analysed. dNdScv was  
792 run using the following parameters; max\_coding\_muts\_per\_sample=5000 and  
793 max\_muts\_per\_gene\_per\_sample=20. Genes with a qval of <0.05 were considered to be under positive  
794 selection.  
795

796 A second phase of cancer gene mutation analysis was undertaken; identifying mutations in this cohort which  
797 are codified in cancer mutation databases and exhibit characteristic traits of cancer driver mutations; an  
798 approach previously employed in the study of normal tissues<sup>1,2</sup>. In this phase of the analysis we sought to identify  
799 the spectrum and frequency of cancer driver mutations in this cohort. Somatic mutations (SBS and ID) were  
800 collated per-sample from all tissues. Analysis was restricted to protein coding regions and mutations were  
801 filtered using lists of known cancer genes; mutations in samples from intestinal epithelium were filtered using a  
802 list of 90 genes associated with colorectal cancer and includes variants that are commonly identified in small  
803 bowel adenocarcinoma<sup>3</sup>; samples from all other tissues including blood were filtered using a pan-cancer list of  
804 369 driver genes<sup>62</sup>. Genes were then characterised according to their predominant molecular behaviour;  
805 dominant, recessive or intermediate (those demonstrating aspects of both types of behaviour) using the COSMIC  
806 Cancer Gene Census<sup>63</sup>. All candidate mutations were annotated using the cBioportal MutationMapper database

807 (https://www.cbioportal.org/mutation\_mapper). Mutations meeting the following criteria were considered to  
808 be driver mutations; truncating mutations (those that cause a shortened RNA transcript, nonsense, essential  
809 splice-site, splice region and frameshift ID) in recessively acting genes, known activating hotspot mutations in  
810 dominant (and recessive) genes and lastly mutations that were in neither of the above categories but  
811 characterised by the MutationMapper database as being 'likely oncogenic' were also included in the final driver  
812 mutation catalogue. We also sought to compare the frequency of driver mutations in histologically normal crypts  
813 with MUTYH mutations to those from individuals who do not carry DNA polymerase mutations. Somatic  
814 mutations from 445 normal intestinal crypts<sup>3</sup> were annotated and filtered using the above criteria. Comparison  
815 was made with normal intestinal crypts from this cohort of individuals with MUTYH germline mutations.  
816  
817

### 818 Modified duplex sequencing (NanoSeq)

819 DNA from bulk blood samples from individuals with germline *MUTYH* mutations was extracted as outlined  
820 above. Samples from normal healthy control was obtained and processed using the following method. Whole  
821 blood was diluted with PBS and mononuclear cells (MNC) were isolated using lymphoprepTM (STEMCELL  
822 Technologies) density gradient centrifugation. The red blood cell and granulocyte fraction of the blood was then  
823 removed. The MNC fraction was depleted of red blood cells by lysis steps involving 3 incubations at room  
824 temperature for 20 mins/10 mins/10 mins respectively with RBC lysis buffer (BioLegend). Tissue lymphocytes  
825 were isolated from Peyer's patches in intestinal mucosa using laser capture microdissection and subjected to  
826 protein lysis as outlined above. Cell lysates were processed and whole genome sequenced using the NanoSeq  
827 protocol.  
828

829 Our modified duplex sequencing method, called NanoSeq, relies on blunt-end restriction enzymes to fragment  
830 the genome in order to avoid errors associated to the filling of 5' overhangs and the extension of internal nicks  
831 during end repair after sonication. Our modified method has error rates < 5e-9<sup>50</sup>.  
832

833 Given the uneven frequencies of trinucleotides in the digested genome, the strong filtering of common SNPs  
834 sites (typically occurring at CpG), and the strong dependence of mutation rates on trinucleotide contexts, our  
835 estimates of mutation burdens are normalized and projected onto genomic trinucleotide frequencies.  
836

837 Let  $t$  denote the count of a given trinucleotide of type  $i = 1 \dots 32$ . The frequency of each trinucleotide is calculated  
838 separately for the genome  $f_i^g$  and for the NanoSeq experiment  $f_i^e$  where:

$$841 \quad f_i = \frac{t_i}{\sum_{i=1}^{32} t_i}$$

842 The ratio of genomic to experimental frequencies for a given trinucleotide is:

$$845 \quad r_i = \frac{f_i^g}{f_i^e}$$

846 There are  $j = 1 \dots 6$  classes of substitution where the mutated base is a pyrimidine. Let  $s_{ij}$  denote the count of  
847 substitution  $j$  in trinucleotide context  $i$ , giving a total of 96 substitution classes. Each substitution count is  
848 corrected as follows:

$$851 \quad s'_{ij} = s_{ij} r_i$$

852

853 The corrected substitution counts provide a substitution profile projected onto the human genome, and are also  
854 used to calculate the corrected mutation burden:

855

856 
$$\beta' = \frac{\sum_{i=1}^{32} \sum_{j=1}^6 s'_{ij}}{\sum_{i=1}^{32} t_i}$$

857

858 Software used in this study is publicly available at the following locations. Mutation calling algorithms are  
859 available at <https://github.com/cancerit>. Code for filtering mutation calls is available  
860 at [https://github.com/TimCoorens/Unmatched\\_NormSeq](https://github.com/TimCoorens/Unmatched_NormSeq). Software for mutational signature analysis is  
861 available at <https://github.com/nicolaroberts/hdp>  
862 , <https://github.com/kgori/sigfit> and <https://github.com/AlexandrovLab>. Software for analysis of duplex /  
863 NanoSeq data is provided at <https://github.com/cancerit/NanoSeq>. Parameters used for these various pieces of  
864 software have been included in the manuscript methods section and supplementary information.

865

866

867 **Data Availability**

868 DNA sequencing data are deposited in the European Genome-Phenome Archive (EGA) with  
869 accession code: EGAD00001007958 and EGAD00001007997.

870

871 The cBioPortal MutationMapper database was accessed at:

872 [https://www.cbioportal.org/mutation\\_mapper?standaloneMutationMapperGeneTab=ATM](https://www.cbioportal.org/mutation_mapper?standaloneMutationMapperGeneTab=ATM)

873

874

875 **Code Availability**

876 Code/software required to reproduce the analyses in this paper are available online and are listed in  
877 Methods.

878

879 **ACKNOWLEDGEMENTS**

880 We thank the staff of Wellcome Sanger Institute Sample Logistics, Genotyping, Pulldown, Sequencing  
881 and Informatics facilities for their contribution including Laura O'Neill, James Hewinson, Yvette Hooks,  
882 Stephen Gamble, Calli Latimer and Kirsty Roberts for their support with sample management and  
883 laboratory work. In addition; Moritz Gerstung and Harald Vöhringer for help with analysis, advice  
884 and discussions. James Chan (Cambridge University Hospitals) and Geraint Williams (Cardiff  
885 University) for assistance with histopathological review. We thank the clinical and research  
886 administration teams at recruitment sites for their assistance with sample collection and patients and  
887 their families for their time as study participants.

888

889 **FUNDING**

890 This work was supported by the Wellcome Trust [206194]. P.S.R. is supported by a Wellcome Clinical  
891 PhD fellowship. Sample collection and research governance were supported by grants to Wales Gene  
892 Park from Health and Care Research Wales (H.C.R.W.). L.E.T. was supported by a postdoctoral  
893 Fellowship from HCRW and H.D.W. by a postdoctoral Fellowship from Ser Cymru.

894

895 **AUTHOR CONTRIBUTIONS**

896 P.S.R., M.R.S., J.R.S. and L.T. conceived the study design. J.R.S., L.T., F.L., L.B., N.L., H.D.W., R.B-S., S.R,  
897 R.t.H., N.C., S.J.A.B. and K.S.P. recruited individuals, collected samples and curated sample and clinical  
898 data. P.S.R., B.C.H.L. and S.V.L. undertook laboratory work. F.A., I.M., S.V.L., L.M.R.H., T.H.H.C. and  
899 M.A.S. developed bespoke DNA library preparation, sequencing and bioinformatic methods. F.A., I.M.,  
900 L.M.R.H., H.L.S. and S.O. contributed and analysed control data. P.S.R., F.A., I.M., S.O. and H.J.  
901 performed data analysis. M.R.S., P.J.C. and I.M. oversaw statistical analysis. M.R.S. and J.R.S. oversaw  
902 the study. All authors were involved in the preparation and review of the manuscript.

903

904 **COMPETING INTERESTS**

905 P.J.C. is a founder, consultant, and stockholder of Mu Genomics Ltd.

906